Sedimentary and structural evolution of the Eastern South Korea Plateau (ESKP), East Sea (Japan Sea)

Senay Horozal[a,*], Gil-Young Kim[a], Deniz Cukur[a], Jang-Jun Bahk[b], David Buchs[c], Byong-Jae Ryu[a], Gwang Hoon Lee[d], Seong-Pil Kim[a]

[a]Korea Institute of Geoscience and Mineral Resources, Daejeon, Republic of Korea

[b]Chungnam National University, Daejeon, Republic of Korea

[c]School of Earth and Ocean Sciences, Cardiff University, United Kingdom

[d]Pukyong National University, Busan, Republic of Korea

*Corresponding author

124 Gwahag-ro, Yuseong-gu, Korea Institute of Geoscience and Mineral Resources, Daejeon, Republic of Korea

Tel.: +82 42 868 3166

Fax: +82 42 868 3417

E-mail address: shorozal@kigam.re.kr

Abstract

The East Sea (Japan Sea) is a semi-enclosed back-arc basin that is thought to preserve a significant record of tectonic evolution and paleo-climatic changes of Eastern Asia during the Neogene. We use here 2-D regional multi-channel seismic reflection profiles and borehole data from Expedition 346 of the Integrated Ocean Drilling Program (IODP) to provide new constraints on the geological history of the Eastern South Korea Plateau (ESKP). The ESKP represents a structurally-complex basement high in the southwestern East Sea which formed during rifting of the back-arc basin. Our new observations show that the ESKP is composed of numerous horsts and grabens controlled by NE-trending normal faults. The acoustic basement is blanketed by Oligocene to recent sediments that have preferentially accumulated in topographic lows (up to 1.5 km thick) and have been cored during Expedition 346 at Site U1430 close to the southern margin of the ESKP. Seismic profiles in the ESKP reveal three units separated by regional unconformities. These seismic units closely correspond to IODP lithostratigraphic units defined at Site U1430, where biostratigraphic data can be used to constrain the timing of three main evolutionary stages of the ESKP. Stage 1 was related to rifting in the late Oligocene and middle Miocene, terminated by a regional uplift leading to an erosional phase in the middle Miocene. Stage 2 was associated with subsidence in the middle and late Miocene and uplift and accompanying erosion or non-deposition in the latest late Miocene. Stage 3 (Pliocene to present) recorded overall uniform hemipelagic-pelagic subsidence of the ESKP with short-lived tectonically-induced uplifts in the late middle Miocene and latest Miocene-early Pliocene. The three stages of evolution of the ESKP closely correlate to sedimentary changes since the Oligocene and suggest a direct control of regional/local tectonics on sedimentation patterns in the southwestern East Sea, with secondary influence of regional climatic and paleo-oceanographic processes.

Keywords: Eastern South Korea Plateau (ESKP), sedimentary and tectonic evolution, seismic reflection data interpretation, IODP Expedition 346, Site U1430, East Sea (Japan Sea)

1. Introduction

Back-arc basins represent an integral but often neglected part of the subduction factory and are thus a major research focus for better understanding tectonics, climatic changes, and magmatic activity along convergent plate margins (Schellart et al., 2003). The occurrence of an extensional regime adjacent to an area of major convergence is not easily explained by the plate tectonics theory (Schellart et al., 2003). Moreover, the reasons why not all subduction systems develop back-arc extension have never been adequately addressed (Sdrolias and Müller, 2006). Shedding light on this and related problems like back-arc initiation and development together with back-arc volcanism is best carried out in places where these tectonic elements and processes are well-preserved. The East Sea (Japan Sea) represents an excellent location to study continental extension and rifting because abundant syn- and post-rift sediments have accumulated in this area (e.g., Kim et al., 2015). Moreoever, thick sedimentary fills of the East Sea preserve a significant record of the paleoceanographic and climatologic evolution of East Asia since the Oligocene (e.g., Tada et al., 2015).

The East Sea is a semi-enclosed back-arc basin located along the eastern margin of the Eurasian Plate and west and northwest of the Philippine Sea and Pacific plates (Fig. 1). The East Sea can be subdivided into three basins that developed in response to continental rifting and seafloor spreading between the early Oligocene and middle Miocene (Tamaki et al., 1992): the Japan Basin (JB), the Yamato Basin (YB), and the Ulleung Basin (UB) (Fig. 1). These three major basins are separated by continental remnants, among which the largest are the Yamato Ridge (YR) in the central part of the East Sea and the North Korea Plateau (NKP) and the South Korea Plateau (SKP) in the west (Fig. 1). The SKP lies at the northern part of

the Ulleung Basin and is further divided into the Eastern South Korea Plateau (ESKP) and the Western South Korea Plateau (WSKP) that are separated by the North Ulleung Trough (NUT in Fig. 2; Chough et al., 2000).

The stratigraphy, timing and style of the extensional deformation of the WSKP have been extensively studied based on seismic reflection profiles (Kim et al., 2007; Kwon et al., 2009; Cukur et al., 2015). Large faults and rift systems on the plateau are attributed to major tectonic events reflecting different stages of evolution of the East Sea (Kim et al., 2007). Sedimentary deposits overlying the acoustic basement vary in thickness from less than 50 m on top of basement highs to over 1,300 m in the basement lows in the WSKP (Cukur et al., 2015). In contrast, the structural and stratigraphic evolution of the ESKP has yet to be characterized in detail.

Oligocene and younger sedimentary deposits in the East Sea have been the focus of several international drilling expeditions (e.g., ODP Legs 127 and 128; Pisciotto et al., 1992; Tamaki et al., 1992). For example, nine drill sites were drilled during IODP Expedition 346 in 2013, with the main goal to reconstruct the Neogene-Quaternary evolution of the Asian monsoon on a millennial time scale and its link to the uplift of the Himalayan and Tibetan plateau (Tada et al., 2015). Site U1430 of Expedition 346 on the southern upper slope of the ESKP offers a valuable opportunity to better characterize the tectonic and paleo-environmental evolution of the South Korea Plateau in close proximity to the Ulleung Basin (Fig. 1). Shipboard observations during Expedition 346 shows that sedimentation at Site U1430 has been dominated by pelagic and/or hemipelagic biogenic deposits with minor volcanic (tephra) and terrigenous (clay to sand) input since the Miocene (Tada et al., 2015). Major changes in lithology such as the presence of centimeter- to meter-scale alternations of dark and light layers at Site U1430 since the Miocene largely reflect local and eustatic sea level changes, climate oscillations, and volcanic and diagenetic processes in the East Sea. In

particular, those lithological alternations reflect millennial-scale variations which are possibly associated with Dansgaard-Oeschger (D-O) cycles (Tada and Irino 1999; Tada et al., 2015). Here, we provide new structural and stratigraphic constraints on the evolution of the ESKP that suggests strong links primarily to local/regional tectonics.

The main objective of this paper is to provide new constraints on the long-term evolutionary stages of the East Sea, focusing on the relative significance of tectonic processes versus climatic changes influencing sedimentation patterns. This approach is intended to improve our understanding of the geological evolution of sedimentary basins at passive margins located in convergent settings. To achieve that goal, the structure and stratigraphy of the ESKP are documented using multi-channel seismic reflection data with the help of biostratigraphic age, lithostratigraphy and digital log data retrieved during the IODP Expedition 346. The seismic sequences and their boundaries are tied to the data from the Site U1430 (see Fig. 2 for location) to form a chronostratigraphic framework of depositional sequences.

2. Geological and oceanographic setting

The opening of the East Sea initiated in the early Oligocene (ca. 32 Ma) in the northeastern Japan Basin (Tamaki et al., 1992), followed by seafloor spreading in the late Oligocene (ca. 28 Ma). While seafloor spreading continued in the Japan Basin, the southern East Sea underwent crustal extension, accompanied by the rotation of the northeastern and southwestern Japan Island Arcs, thereby forming the Yamato and Ulleung basins (Tamaki et al., 1992). In the middle Miocene (ca. 15 Ma), changes in plate motions and subduction mode along the subduction zones of eastern and southeastern Japan caused crustal shortening and back-arc basins inversion (Lee et al., 2011). This inversion resulted in a series of thrusts and

anticlines in the southern margin of the Ulleung Basin. Subsidence has been taking place in the Ulleung Basin since the end of late Miocene (Lee et al., 2011).

The seafloor of the Ulleung Basin is about 2,200 m deep in the northern part and generally smooth except for a few volcanic seamounts and sills (Fig. 1). The SKP, which is one of several large submarine continental remnants in the East Sea, occupies the northern part of the Ulleung Basin (Fig. 1). The eastern component of the SKP, which is the focus of our study, has an area of about 11,000 km^2 and lies in water depths of 700 to 2,000 meters. The plateau has a roughly circular shape, extending about 350 km E-W and 260 km N-S. The plateau is bordered by the Ulleung Interplain Gap (UIG), also known as the Korea Gap (KG), in the southeast, the WSKP in the west, and the Japan Basin in the north. Dredging (see Fig. 1A for locations) showed that the SKP basement is composed of early Cretaceous metamorphic rocks (ca. 102–110 Ma) (Lelikov and Bersenev, 1975). Refraction studies in the SKP (Kim et al., 2015) revealed uniform crustal thicknesses of about 15 km across the whole plateau. The UIG is approximately 90 km long and over 2500 m deep (Fig. 2). Multibeam bathymetric data clearly shows a number of channels and channel-like features which appear to merge into the UIG (Lee et al., 1996). They are erosional in origin and probably associated with strong bottom currents flowing through the UIG (Lee et al., 1996).

The modern East Sea is vertically stratified in two water masses: surface layer and deep layer (Lee et al., 2008). The surface water circulation is dominated by the Taiwan Warm Current (TWC) which forms the western branch of the Kuroshio Current (KC). The TWC generally carries warm (26 ºC in summer and 14 ºC in winter) and saline water to the sea, with a mean velocity of about 10-90 cm/s (Teague et al., 2002). Estimates of the transport of this inflow vary considerably, but the annual mean transport is 2 x 106 m^3 s^{-1}, with a minimum transport in winter and spring (Church et al., 2005). The TWC enters the East Sea through the Korea Strait and splits into three major branches (labeled as TWC-1, TWC-2, and

TWC-3; Fig. 1). The most westward stream, TWC-3, flows northward along the coast of Korea up to 37-38°N and then turns eastward and passes through the SKP (Fig. 1). The other two major currents, TWC-1 and TWC-2, flow northward along the eastern Japanese margin and exit the sea mostly through the Tsugaru and Soya straits (Fig. 1; Isobe, 1999). The nearly homogeneous deep water is cold (0–1 ℃) and well-oxygenated (5–6 ml/l) (Kim et al., 1996; Itaki et al., 2004; Kang et al., 2004; Lee et al., 2008). The cold deep water seems to be formed in the northwestern East Sea because of strong cooling of surface water and sea ice formation during winter (Lee et al., 2008).

3. Datasets and methods

Data used in this study consists of: (1) about 2,500 km of multi-channel seismic reflection profiles acquired by the Korea Institute of Geosciences and Mineral Resources (KIGAM) (Fig. 2A), and (2) natural gamma-ray (NGR), acoustic and density logs as well as lithostratigraphic and biostratigraphic data (Fig. 3), and X-ray diffraction (XRD) data from the IODP Expedition 346 Site U1430. The multi-channel seismic reflection survey was carried out in 2004 by *R/V Tamhae II*. An 80-channel, 1,000 m streamer recorded shots from a 20.5-1/2,000 psi source array. The shot interval was 25 m. Systematic data processing at KIGAM included: geometry definition and CMP sorting, 1st minimum phase bandpass filter, signature deconvolution, gap deconvolution, 2nd minimum phase bandpass filter, normal moveout, true amplitude recovery, semblance velocity analysis, full-offset stack and post-stack migration. IHS Kingdom Suite (version 8.5) software was used for seismic data interpretation and mapping.

Acoustic and density logs at the IODP Hole UB1430B were used to generate synthetic seismograms for synthetic-to-well tie that helped to obtain time-depth conversions. Synthetic traces were generated by convolving the reflectivity from the density and acoustic logs and the source wavelet extracted from the seismic data at the well location (Table 1). Then, each

pick from the synthetic trace was correlated to those in the seismic profiles (red color). Next, the time-depth relationship at the well location was estimated by synthetic-to-well tie and applied to the entire 2-D seismic data set. All main events of synthetic seismograms in Table 1 correlate well (correlation coefficient up to 80%) with seismic traces. As the logs extend to only between 80 to 260 meters below seafloor (mbsf), the remaining time-depth information was extrapolated automatically by the software. Hence, estimation errors could possibly occur in conversion from 1-D (well) data to 3-D (seismic) configuration. Geologic ages of key unconformities at the Site U1430 were taken from the preliminary scientific report (Tada et al., 2015). The maximum sedimentation rates for each seismic megasequence were estimated from the sediment thickness at the depocenter and the age ranges of each megasequence.

4. Results

We identified three major unconformities or sequence boundaries across the plateau (Figs. 3-10) as well as faults which are predominantly normal basin-deep and secondary shallow faults. The unconformities are characterized by high-amplitude reflections forming truncations, onlap and/or downlap surfaces on 2-D seismic reflection data. The unconformities or megasequence boundaries (MB) and the megasequences (MS) are referred to as MB1 to MB3 and MS1 to MS3, respectively, from oldest to youngest. Each MS rests on its corresponding MB.

4.1 Regional Unconformities

4.1.1 MB1 or top of acoustic basement (Early Cretaceous)

MB1 or the top of the acoustic basement has been consistently mapped throughout the study area (Figs. 3-10). Acoustically, it is picked as the deepest coherent reflector above a featureless basement. The basement of the ESKP is formed by blocks and appears to be significantly faulted, while the basement in the UIG is relatively unfaulted (Figs. 3-10). In the

south of the ESKP, there are a number of prominent volcanic seamounts, which extend above the level of basement and form bathymetric highs (Fig. 5). In the eastern and southeastern parts of the ESKP, the upper surface of MB1 appears to be rather flat (i.e., Figs. 6 and 7).

The depth structure map of MB1 shows that the ESKP is dominated by a horst and graben morphology, with numerous half-grabens 10-15 km wide (Fig. 11A). Several prominent normal faults are also evident on the depth structure map; most of them exhibit a SW-NE orientation, while a few (about 10%) of them trend E-W (Figs. 3-11). The displacement of the basement-bounding (main) normal faults on the flanks of structural highs and those dipping through the UIG (Figs. 4-8) are generally over 2 km. Several basement ridges and troughs were bounded by these normal faults that were shaped by extension and rifting (Fig. 15A). Basement-bounding normal faults forming small grabens and smaller (secondary) normal faults, which do not extend through younger megasequence boundaries, displace with a slip about less than a kilometer (Figs. 4-10). The depth of the MB1 increases generally from the northwest to the southeast (Fig. 11A). MB1 lies at total depths lower than 1,200 m in the northwestern part of the plateau, deepening over 4,200 m through the UIG and further towards the northwest. Two prominent volcanic seamounts are also identified in the UIG.

4.1.2 MB2 (Late Middle Miocene; ca. 13 Ma)

MB2, which is dated the late Middle Miocene (ca. 13 Ma), forms a prominent unconformity in the ESKP (Figs. 3-10). It is characterized by a high-amplitude reflection on seismic profiles and generally onlaps onto basement highs or terminates against the large basement faults (Fig. 8). MB2 forms a conformable surface within the basement lows and is characterized by erosional truncation over the tilted basement highs (Fig. 8). Most of secondary normal faults that displaced MB1 die out immediately below the MB2 (Fig. 9). The faults cutting MB2 have smaller offsets on the order of tens to hundreds of meters than those

displacing MB1 (Figs. 4-10). MB2 forms a wedge-shape at the dip of main faults (i.e., Fig. 8B). This unconformity has been intersected at the IODP Hole U1430B (Fig. 3); Middle Miocene siliceous claystones and glauconitic sandstones were recovered below the unconformity and Late Miocene diatom oozes above the unconformity. The depths of MB2 range from less than 1,300 m on the north and northwestern parts to over 2,300 m below sea level on the southwestern and east-northeastern parts of the plateau (Fig. 11B).

4.1.3 MB3 (Latest Late Miocene; ca. 7 Ma – 4.5 Ma)

MB3 represents a major regional unconformity that extends over much of the plateau (Figs. 3-10). It is dated as the latest Late Miocene and marks a major hiatus that extends from ca. 7 Ma to ca. 4.5 Ma (Tada et al., 2015). Seismically, it is characterized by a high-amplitude reflection (Figs. 8 and 9) and is relatively conformable with overlying reflectors. In other areas, on the steep flanks in the eastern part of the plateau, MB3 is characterized by erosional truncations (Figs. 8C and 9C). The depths of the MB3 range from less than 1,000 m in the northwest to over 1,900 m (Fig. 11C) in the east and northeast plateau. The majority of secondary faults do not pierce through MB1 (i.e., Figs. 4-6) and the main faults displacing MB1 have small offsets (Figs. 8 and 9) compared to those cutting MB1 and MB2.

4.2 Megasequences

4.2.1 Megasequence 1 (MS1; Late Oligocene and Late Middle Miocene)

MS1 is the oldest sedimentary unit overlying the basement and is bounded at the top by MB2 which is an angular unconformity with high reflection amplitude (ca. 13 Ma; Figs. 3-10). It is commonly observed in basement lows where it onlaps basement ridges or terminates against basement faults (Fig. 8). It consists of moderate- to high-amplitude, discontinuous reflections with growth geometries against the basement-bounding normal faults (Fig. 8). Locally, this unit appears to be intensely folded and faulted (Fig. 9). MS1 is the thickest of the

three units attaining a thickness of at least 300 m to over 750 m in the plateau's subbasin lows at the west, north and southeast (Fig. 12A). The isopach map also shows that MS1 appears to be affected by basement-controlled faulting as the thickest deposits lie immediately next to large basement faults (Fig. 12A). The maximum sedimentation rate throughout MS1 between ca. 23–13 Ma is about 78 m/m.y. (Fig. 12A).

4.2.2 Megasequence 2 (MS2; Late Middle Miocene and latest Late Miocene)

MS2 has been mapped over large areas of the plateau (Figs. 3-10). It shows onlap relationships against basement highs and fills the lower areas formed by the tilted and folded blocks (Figs. 8 and 9). MS2 also show some thickening toward basement normal faults although less than MS1 (i.e., Fig. 8B). MS2 is characterized by low-amplitude continuous reflections (Fig. 12). Its upper surface is bound by erosional truncations cut off on the MB3 (Fig. 9) that is prominent on the seismic lines across the Plateau. MS2 ranges in thickness from less than 50 m to over 350 m (Fig. 12B) and includes a major depocenter in the southern part of the Plateau. The maximum sedimentation rate throughout the MS2 between ca. 13–7 Ma is approximately 70 m/m.y. (Fig. 12B).

4.2.3 Megasequence 3 (MS3; latest Late Miocene and Present)

MS3 is the youngest sedimentary unit identified on the plateau (Figs. 3-10). It includes onlap-fill seismic facies together with continuous reflections of variable amplitude but generally higher amplitude than MS2 (Figs. 3-10). In the northern part of the plateau, the top of MS3 forms morphological steps through the south (Fig. 9). Basement-bounding normal faults generally do not indicate any growth geometries in unit MS3 as observed in MS2 and MS1. The majority of faults which are not (main) basin-bounding but are secondary normal faults do not penetrate through the MS3 (e.g., Figs. 9-10). MS3 extends as a thin layer (< 50 m thick) over most of the Plateau. It reaches a maximum thickness of 300 m in the main

depocenter at the southeastern part and locally in the southwestern part of plateau (Fig. 12C). The maximum sedimentation rate throughout the MS3 (from ca. 4.5 Ma to the Present) is approximately 80 m/m.y. (Fig. 12C).

4.2.4 Total sediment thickness

Much of the ESKP is covered by sediments, except for some elevated areas where erosion may have prevailed (Fig. 12D). Several major depocenters occur on the ESKP with maximum thicknesses of about 1,000 m. The thickest sedimentary section (> 2,000 m) is found in the UIG. The structure of the basement has clearly played a key role in controlling plateau sedimentation, resulting in deeply infilled depressions and thinly covered elevated areas. The maximum total sedimentation rate in the depocenter (from ca. 23 Ma to the Present) is ~105 m/m.y. (Fig. 12D).

4.3 Sedimentological changes associated with the megasequences

Megasequences based on our regional observations closely correlate with IODP logging data recorded at Site U1430 lithologic units defined during IODP Expedition 346. Unit MS3 includes IODP lithostratigraphic units IA, IB and IIA at Site U1430, for a total thickness of approximately 75 m (Fig. 13; Tada al., 2015). These IODP units are composed of alternating organic-rich and organic-poor silty clay, clayey silt, foraminifer-rich diatom-bearing clayey silt, nannofossil ooze and tephra (Tada al., 2015). IODP subunit IIA marks a transition to subunit IIB (from the base of MS3 to the upper part of MS2), whose upper boundary is defined by increasing diatom content coupled with an overall increase in NGR log values downhole (Tada al., 2015) up to 180 mbsf, which is followed by a decreasing trend until MB2 (Fig. 3). Despite shipboard visual observations, the cores could not confirm the existence of a major stratigraphic break between IODP subunits IIA and IIB, where the MB3 lies in the seismic data. However based on preliminary biostratigraphic data the MB3 boundary would

be related, within biostratigraphic and seismic resolution errors, to a possible hiatus from ca. 7 to 4.5 Ma (Fig. 3 and 13; Tada et al., 2015). The sedimentation rates increased upward throughout Unit MS3; it is approximately 10 m/m.y. from ca. 4.5 to 1 Ma (in IODP subunits IA, IB and IIA), and 45 m/m.y. from ca. 1 Ma to the present (i.e., the uppermost part of subunit IA) (Fig. 13).

Unit MS2 correlates with IODP lithostratigraphic subunits IIB, IIIA and IIIB at Site U1430 (Fig. 13; Tada et al., 2015). This seismic unit has a total thickness of 175 m and is dominated by diatom ooze and diatom-rich/bearing silty clay. Its lower part (IODP subunit IIIB) is composed of siliceous silty clay and claystone, accompanied by a progressive downhole decrease of NGR values, and mark the transition to the distinctively sandier deposits of underlying unit MS1. Unit MS2 deposited with a sedimentation rate of 40 m/m.y. that possibly decreases to less than 10 m/m.y. in transitional subunit IIIB (Fig. 13; Tada et al., 2015).

Unit MS1 was only partly recovered during Expedition 346 and corresponds to IODP unit IV at Site U1430 (Fig. 13; Tada et al., 2015). It overlies the acoustic basement which is further down of hole-end at a depth greater than 500 mbsf with an estimated thickness of over 250 m (Fig. 3). Unit MS1 is predominantly composed of glauconite-quartz-feldspar–rich sandstone with minor tephra layers. Unit MS1 has higher quartz and feldspar contents than the overlying Unit MS2; this observation is also supported by smear slide observations that outline a coarser (silty) terrigenous input in the form of quartz and feldspar grains in Unit MS1 (Tada et al., 2015). Similarly, Unit MS1 has more abundant clay minerals compared to Unit MS2. Unit MS1 generally has higher feldspar content than Unit MS2. Higher plagioclase content at a given quartz content exists in Unit MS1 (i.e., lower quartz/feldspar ratio) compared to other sediments recovered at the Site U1430 (Fig. 14). Lithological

characteristics of units MS3, MS2 and MS1 at IODP Site U1430 are very consistent with XRD semi-quantitative data acquired during Expedition 346 (Figs. 13 and 14).

5. Discussion

Several studies suggest that the sedimentary record preserved in the East Sea offers the opportunity to characterize the paleo-oceanographic and paleo-climatic evolution of East Asia (e.g., Tada, 1994). Tada et al. (2015) propose that the changes in sedimentation observed at Site U1430 could provide significant constraints on a range of atmospheric and oceanographic processes since the middle Miocene. Centimeter- to meter-scale alternations of dark and light layers in the drill cores from the East Sea clearly indicate that climatic control has been effective on a short (< 1 m.yr.) time scale (Tada et al., 2015), but possible effects of tectonics on sedimentological changes in the basin on a longer time scale have remained poorly constrained. Our study of the evolution of the ESKP offers therefore a valuable opportunity to better assess the link between regional tectonics and basin sedimentation.

Our observations clearly indicate that seismic units MS1, MS2 and MS3 closely correlate to significant sedimentological changes during the evolution of the East Sea. Several factors could have controlled these changes, including variations in the supply of continental dust, regional volcanic activity, global sea level, and biogenic productivity/paleo-oceanographic conditions (e.g., Tada, 1994; Tada et al., 2015). However, our detailed seismic analysis shows that these changes were at least partly controlled by tectonics during the development of the East Sea back-arc in the Miocene-Pliocene (Table 2). This is a significant observation that indicates that sedimentological changes on a long time scale in the basin have been influenced (directly or indirectly) by local tectonic activity. Earlier studies also indicate that tectonic activity played an important role in sedimentation in other back-arc basins in the western Pacific (Marsaglia, 1995). For instance, the stratigraphy of the Sulu Basin has

recorded varying sediment input from volcanic and continental sources related to changes in the tectonic setting of the basin (Marsaglia et al., 1995). We present below a model of tectono-sedimentary evolution of the ESKP between the late Oligocene and Pleistocene with three stages that chiefly correspond to the megasequences defined in this study (Fig. 15).

5.1 Stage 1 (late Oligocene-late middle Miocene, ca. 28 Ma–11.8 Ma)

Stage 1 overlaps with the initial rifting and extension of the South Korea Plateau that started in the late Oligocene (Jolivet and Tamaki, 1992; Kim et al., 2007). Extension and rifting in the ESKP led to the formation of several basement ridges and troughs bound by normal faults that are well recorded in the present study (Fig. 15A). These structures are generally associated with tensional tectonics, implying that the ESKP formed by rifting and extension along a series of normal faults. Crustal rifting occurs in a remarkably similar manner between intracontinental, incipient ocean spreading settings and passive continental margins (Wright, 1997). The presence of NE-trending normal faults at the ESKP further indicates that the continental crust here was subjected to NW-SE extension. The tension was probably coeval with the opening of the East Sea and related to the northwesterly subduction of the Pacific Plate beneath the Eurasian Plate (Tamaki, 1988; Kaneoka et al., 1992).

During Stage 1, relatively shallow-water conditions existed on the horsts of the ESKP (Fig. 15A). The shallow-marine environment is also suggested by the paleogeographic reconstruction of the mid-western East Sea based on the recognition of wave planation surfaces (Kim et al., 2013; see their Fig. 12A-B). The site of the UIG was probably deeper than adjoining areas. The syn-rift units of Stage 1 show divergent reflections, suggesting synchronous deposition and faulting. Moreover, the presence of moderate- to- high-amplitude, discontinuous reflections suggests the prevalence of non-marine, mainly fluvial-deltaic sediments, in the plateau during that interval (e.g., Fig. 8). This interpretation is also supported by the occurrence of glauconite-quartz-feldspar–rich sandstone interpreted to have

been deposited in relatively shallow-marine environments (Tada et al., 2015). Unit MS1 generally has higher feldspar content than the MS2, which could reflect changes in sedimentary input from terrigenous-dominant to biogenic-dominant during the Miocene. Higher plagioclase content at a given quartz content in Unit MS1 (i.e., lower quartz/feldspar ratio) compared to other sediments recovered at the Site U1430 indicate a more immature composition of the coarse terrigenous component in this unit (Fig. 14). The coarse, sandy nature of the sediments suggests that they probably represent a detrital input derived from adjacent basement highs (Fig. 3). This interpretation is also supported by the identification of a smooth and flat surface of the basement highs on seismic reflection profiles that is indicative of subaerial erosion or shallow wave ravinement surface due to uplift before subsequent subsidence and sedimentation (Fig. 15A).Similarly, rapid extension and subsidence took place at an early stage of rifting in the WSKP (Cukur et al., 2015). Volcanic activity was widespread at early times and about 700 m thick succession of lacustrine and fluvial sediments was deposited during this period (Cukur et al., 2015).

Klein (1985), on the basis of DSDP cores, documented nine major sediment types from back-arc basin sites in the western Pacific: biogenic carbonates, hemipelagic clays, submarine fan deposits (turbidites), resedimented carbonates, pyroclastic flows, silty basinal turbidites, biogenic silica sediments, pelagic clays, and debris flows. The ODP drilling in the Sumisu Rift, which is an interoceanic back-arc basin behind the Izu-Bonin arc, encountered thick, coarse pumiceous units deposited by sediment-gravity flows (Taylor, 1992). In the Sulu back-arc basin, between northern Borneo and the Philippines, the early basin fill contains coarse-grained volcaniclastic sediments deposited by a series of submarine gravity flows and turbidity currents fed by voluminous explosive eruptions (Rangin et al., 1990). Hence, the early part of basin fill in the intraoceanic back-arc basins may be dominated by mass-transport processes that carry clastic and pyroclastic materials into the basin (Einsele, 1992). The high-

energy sedimentary processes were also probably common during the earlier history of the ESKP, similar to the intraoceanic back-arc basins.

The extension and subsidence of the ESKP were punctuated by uplift during the latest middle Miocene (ca. 13 Ma). The seismic data clearly shows local folding of MS1 sedimentary unit (Figs. 10 and 12). The truncation at MB2 over the structural high (i.e., Figs. 5 and 8B-C) indicates tilting of fault blocks and subsequent erosion. Thus, MB2 could mark the end of the extensional phase over the plateau at ca. 13–11.8 Ma. Evidence of regional uplift (10-100 m/m.y.) also appears in the western East Sea at ca. 11–10 Ma with compressional uplift and destruction of sub-basins in arc and arc-flank areas of Honshu, Hokkaido, and Sakhalin (Ingle, 1992). This regional compressional regime is also evidenced by folding and thrust faulting in the southern margin of the Ulleung Basin (Lee et al., 2011). This tectonic event is related to the changes in plate motions and subduction mode along the subduction zones, east and southeast of the Japanese Islands (Lee et al., 2011). Lee et al. (2011) further attributed the tectonic switching from extension to compression to the flat subduction of the incoming Shikoku Basin lithosphere. The convergence of young, hot and buoyant oceanic lithosphere with continental lithosphere may induce low-angle or flat subduction, causing strong interplate coupling (Uyeda, 1991; Gutscher, 2001) that leads to tectonic switching from extension to compression along the margin of the overriding plate (Gutscher et al., 2000; Collins, 2002). The compressional deformation is particularly prominent along the southern margin of the East Sea (Itoh et al., 1997; Lee and Kim, 2002; Lee et al., 2011). In contrast, the WSKP underwent a second phase of E-W extension during this period (Cukur et al., 2015). It might well be that this compressional deformation did not propagate or jump to the WSKP and to the eastern margin of Korea. Yoon (1994), analyzing the high-resolution seismic reflection profiles, did not recognize any compressional features across the eastern Korean continental margin during that time.

5.1 Stage 2 (middle Miocene-upper Miocene, ca. 11.8 Ma–4.5 Ma)

Stage 2 represents a phase of relative tectonic quiescence along the plateau (Fig. 15B). During this period, there were no significant tectonic perturbations in most of the ESKP, so the sedimentary strata in the depressions are generally horizontal and undeformed except locally by minor faulting. A lack of regionally faulted angular unconformities or tectonically enhanced unconformities during this stage suggests that the plateau has subsided rather monotonously without any significant uplift or thermal perturbation. This stage also witnessed the establishment of marine conditions over the entire plateau. During this time, thick marine sediments (hemipelagic sequences; up to 400 m in Fig. 12B), which are recorded by low-amplitude continuous reflections on seismic profiles, infilled the grabens and half grabens and draped the basement highs (Figs. 4-10). The deep marine environment during this period is also supported in the drill cores by the occurrences of diatomaceous silty-clay, diatom ooze, siliceous silty-clay and claystone (Tada et al., 2015). The composition of marine sediments at the Site U1430 changed from terrigenous-rich to biogenic-rich at the onset of Stage 2, which likely resulted from the total submergence of topographic highs on the plateau and the restricted supply of proximal terrigenous material.

Evidence for increased water depths at this time is found in different parts of the East Sea. For instance, this phase in the WSKP is characterized by the establishment for the first time of marine conditions over the entire plateau (Cukur et al., 2015). Moreover, Chough and Barg (1987), on the basis of the distribution of benthic foraminifers, suggest that maximum water depths ca. 1800 m were achieved during the middle Miocene in the southern margin of the Ulleung Basin. Ingle (1992) proposed that rapid subsidence in the middle Miocene was related to the pull-apart opening of the East (Japan) Sea basins. The presence of sheet-draping reflections may further indicate post-rift subsidence at the ESKP that could have been induced by thermal cooling of the asthenospheric mantle (Kim et al., 2015). In addition, higher sea

levels during this period also correlate well with the global sea level chart (Haq et al., 1987; Berggren et al., 1995; Table 2).

The end of Stage 2 was marked by a major unconformity and a possible hiatus (ca. 7–4.5 Ma) of unclear origin. Previous studies also show that the IODP Site U1430 is under the influence of the second branch of the Taiwan Warm Current (TWC-2 in Fig. 1) (Isoda, 2011), whereas the third branch of the Taiwan Warm Current (TWC-3) passes through WSKP. Hence, sediments deposited during this interval could have been eroded by bottom currents. Seismic reflection profiles along the steep flanks of the plateau show truncated sedimentary layers (e.g., Fig. 9).

The Late Miocene-Pliocene hiatus may also be attributed to a short-lived, tectonically-induced uplift of the plateau that could have led to strong current sweeping of certain seafloor areas. This tectonic activity is evidenced by tilted and eroded layers of MS2 on the seismic sections (Figs. 8B and 9B) and may have been associated with the eastward movement of the Amur Plate during the Pliocene (Taira, 2001). According to Lee et al. (2011), a sudden inversion occurred at ca. 5.5 Ma in the southwestern margin of the East Sea as a result of the eastward movement of the Amur Plate which may be related to far-field stresses imposed by the India-Eurasia collision (Park et al., 2006) or the reactivation of rifting in the Baikal zone (Taira, 2001). The present-day stress field in East Asia, interpreted from focal mechanism solution of recent earthquakes, shows also a strong eastward component (Park et al., 2006; Choi et al., 2012). Although we cannot verify the primary cause of the hiatus, seismic and sedimentological data strongly suggest a profound change in environmental conditions and biological activity in the water column and on the seafloor at ca. 7–4.5 Ma that increased the restriction of the marginal sea. Non-deposition and/or erosion could have been associated with the uplift of the plateau into depths that could also be affected by strong bottom currents around the UIG (Chang et al., 2009; Kim et al., 2013).

Intense compression also occurred in the western margin of the WSKP in the latest Miocene, leading to the development of a series of gentle anticlines and reverse faults (Cukur et al., 2015). Moreover, some of the old half-graben systems in the WSKP appear to have been inverted at this time. We do not, however, observe any thrust and reactivated faults in the ESKP which are common in the western edge of the WSKP (Cukur et al., 2015). This is probably because the E-W compressive stress resulted from eastward movement of the Amur Plate could easily have been accommodated by reverse and strike-slip motions along the preexisting normal faults bounding the WSKP and other basement highs along the eastern Korea margin.

5.3 Stage 3 (Pliocene to Present, ca. 4.8 Ma– Present)

Hemipelagic sedimentation and continued subsidence of the ESKP since the Pliocene has allowed the formation of a sediment blanket (Fig. 15C). Unit MS3 has higher contents in quartz and feldspar than those of the underlying Unit MS2; this observation is also supported by smear slide observations that outline a coarser (silty) terrigenous input in the form of quartz and feldspar grains in Unit MS3 (Tada et al., 2015). Similarly, Unit MS3 has more abundant clay minerals compared to Unit MS2, which could be due at least in part to alteration of tephra layers deposited post MB2.

Bottom currents appear to become dominant at the base of the outer margin of the plateau where it meets the UIG (Figs. 4, 7 and 15C); here, much of the thick sequence has been eroded by currents. Bottom current activity in the UIG has also been inferred from the multibeam bathymetric data that show a number of channels or channel-like features on the seafloor (Lee et al., 1996). The Holocene East Sea circulation model by Seung and Yoon (1995) also suggests the presence of deep currents in the UIG that flow from the Ulleung Basin into the Japan Basin. The role of bottom currents in sediment deposition and

distribution in the UIG needs a further detailed study for a better understanding of the sedimentary history and paleoceanographic changes of the East Sea.

Volcanoes in the adjacent margins also appear to have been active at this time, as several tephra deposits were found in drilled cores (Tada et al., 2015). Overall, Stage 3 is almost devoid of major faulting, suggesting that the area has been relatively stable for the last 4.5 Ma. Subsidence has been dominant in the WSKP as similar to the ESKP since the early Pliocene, which was locally interspersed by inversion along the reactivated normal faults (Cukur et al., 2015). Because the eastward compression still dominated in the eastern Korean margin (Choi et al., 2012), this inversion that affected the western corner of the WSKP is likely to be result of compression that began after 5.5 Ma (Lee et al., 2011). The absence of recent inversion structures in the eastern part of WSKP and in the ESKP might be explained by the presence of structural highs in eastern continental margin of Korea. These highs could have acted as structural barriers for transporting compressive forces into the deep basinal areas. Hence, much of the contractional stress at this time appear to have been accommodated along the pre-existing normal faults, located immediately next to the major structural highs (Cukur et al., 2015, in their Fig. 12).

The apparent dominance of mass-transport deposits in the WSKP further suggests that the sedimentation pattern in the WSKP was quite different from that of the ESKP where hemipelagic sedimentation has prevailed throughout the Stage 3. This is not surprising as the ESKP was protected from mass-transport deposits due to its elevated location. The maximum sediment thickness in the WSKP is about 2 times higher than that in the ESKP, mainly due to the abundance of mass-transport sediments deposited in the WSKP.

6. Summary and Conclusions

Regional multi-channel seismic reflection profiles together with drilling data provide a new insight to the geologic evolution of the Eastern South Korea Plateau (ESKP). Numerous graben and half-grabens are documented along the ESKP, which formed in response to a phase of NW-SE extension between the late Oligocene and middle Miocene (28–13 Ma). During this period, shallow-water conditions prevailed in the basement depressions and terrigenous sediments derived from adjacent basement highs filled these depressions. At ca. 13 Ma, the extension was terminated by a regional uplift which might be associated with a regional tectonic inversion in the East Sea. Between ca.13 Ma and ca. 7 Ma, fairly more tectonically-stable conditions existed and hemiplegic sediments dominated the ESKP. This time also marks the development of fully marine conditions in the area. Non-deposition and/or erosion between 7–4.5 Ma could have been associated with the uplift of the plateau into depths prone to stronger bottom currents. The cause of the uplift was probably the eastward movement of the Amur Plate to the east of the area. Finally, subsidence resumed from the Pliocene until Present, with local erosion by bottom currents along the escarpments of the plateau that border the UIG. The relatively undisturbed nature of the sediments indicates a long-term passive nature of plateau. Our study, therefore, documents a close link between the lithostratigraphic and tectonic evolution of the ESKP. These results suggest that the morphological evolution of the plateau, probably controlled by regional tectonics of the East Sea, could have played an important role in local sedimentation patterns since the Oligocene. Although the sediment record in the basin can provide significant constraints on paleo-oceanographic/climatic processes on a long-time (>1 m.yr.) scale, the spatial and temporal scales of tectonic effects in the East Sea will have to be determined in detail to fully comprehend the nature of this record.

Acknowledgments

This study was carried out as part of the project entitled “International Ocean Discovery Program” (grant number: 16-9852) supported by the Ministry of Oceans and Fisheries, Korea and the project entitled “Marine Geological and Geophysical Mapping of the Korean Seas” (grant number: 16-3317) supported by the Ministry of Knowledge Economy (MKE; currently Ministry of Trade, Industry and Energy: MOTIE). The scientists, and responsible staffs and crew of the research vessel *R/V Tamhae II* worked during data acquisition are greatly appreciated. We thank M. Rabineau and an anonymous reviewer, and the associate editor, F. J. J. Lobo, for their valuable comments. The geological software IHS Kingdom Suite (version 8.5) was used for seismic data interpretation.

References

Berggren, W.A., Kent, D.V., Swisher, C.C., and Aubry, M.-P., 1995. A revised Cenozoic geochronology and chronostratigraphy, in Berggren, W.A., et al., eds., Geochronology, time scales and global stratigraphic correlations: A unified temporal framework for an historical geology: SEPM (Society for Sedimentary Geology) Special Publication 54, p. 129–212.

Chang, K.-I., Kim, K., Kim, Y.-B., Teague, W.J., Lee, J.C., Lee, J.-H., 2009. Deep flow and transport through the Ulleung Interplain Gap in the Southwestern East/Japan Sea. Deep-Sea Research Part I: Oceanographic Research Papers 56 (1), 61–72.

Choi, H., Hong, T.K., He, X. et al., 2012. Seismic evidence of reverse activation of a paleo-rifting system in the East Sea (Sea of Japan). Tectonophysics 572–573, 123–133.

Chough, S.K., Barg, E. 1987. Tectonic history of Ulleung basin margin, East Sea (Sea of Japan). Geology, 15, 45–48.

Chough, S.K., Lee, H.J., Yoon, S.H., 2000. Marine geology of Korean Seas. New York: Elsevier, p. 313.

Church, A.J., Benthoux, J.-P. and Alexander, A., 2005. Semienclosed Seas, Islands and Australia Coastal Segment. In: The Global Coastal Ocean: Multiscale Interdisciplinary Processes, [Eds. Robinson, A.R. and Brink, K.H.] The Sea: Ideas and Observations of Progress in the Study of the Seas 11, Regional Studies and Synthesis, 87-89. Harvard University Press. Cambridge, Massachusetts and London, 1067 pp.

Collins, W.J., 2002. Hot orogens, tectonic switching, and creation of continental crust. Geology 30, 535−538.

Cukur, D., Kim, S.-P., Horozal, S., Ryu, B.-J., Kim, G.-Y., Kong, G.-S., 2015. Seismic stratigraphy and structural analysis of the western South Korea Plateau (WSKP), East Sea. Quaternary International 384, 1-15. DOI: 10.1016/j.quaint.2015.05.023.

Einsele, G., 1992. Sedimentary Basins. Berlin, Heidelberg, New York: Springer-Verlag. 628 pp.

Gutscher, M.A., Sparkman, W., Bijwaard, H. et al., 2000. Geodynamics of flat subduction: seismicity and tomographic constraints from the Andean margin. Tectonics 19, 814−833.

Gutscher, M.A., 2001. An Andean model of interplate coupling and strain partitioning applied to the flat subduction zone of SW Japan (Nankai Trough). Tectonophysics 333, 95−109.

Haq, B.U., Hardenbol, J., and Vail, P.R., 1987. Chronology of fluctuating sea levels since the Triassic (250 million years ago to present). Science 235, 1156–1167.

Ingle, J.C., Jr., 1992. Subsidence of the Japan Sea: Stratigraphic evidence from ODP sites and onshore sections. In: Tamaki, K., Suyehiro, K., Allan, J., McWilliams, M., et al. [Eds]; Proceedings of Ocean Drilling Program, Scientific Results 127/128 Part 2, College Station, Texas: Ocean Drilling Program, pp. 1197–1218.

Isobe, A., 1999. On the origin of the Tsushima Warm Current and its seasonality. Cont. Shelf Res. 19, 117–133.

Isoda, Y., 2011. Climate change and physical process associated with the Tsushima Warm Current. *Mem. Fac. Fish. Sci., Hokkaido Univ.,* 53(2):2–12. http://hdl.handle.net/ 2115/47547.

Itaki, T., Ikehara, K., Motoyama, I., Hasegawa, S., 2004. Abrupt ventilation changes in the Japan Sea over the last 30 yr: evidence from deep-dwelling radiolarians. Palaeogeography, Palaeoclimatology, Palaeoecology 208, 263–278.

Itoh, Y., Nakajima, T., Takemura, A., 1997. Neogene deformation of the back-arc shelf of Southwest Japan and its impact on the palaeoenvironments of the Japan Sea. Tectonophysics 281, 71−82.

Jolivet, L., & Tamaki, K., 1992. Neogene kinematics in the Japan Sea region and the volcanic activity of the Northeast Japan arc. Site 794. Proceedings of Ocean Drilling Program, Scientific Results, Vol. 127/128, Part 2, College Station, Texas: Ocean Drilling Program, pp. 1311–1331.

Kaneoka, I., Takigami, Y., Takaoka, N., Yamashita, S., Tamaki, K., 1992. ^{40}Ar-^{39}Ar analysis of volcanic rocks recovered from the Japan Sea floor: Constraints on the age of formation of the Japan Sea. In: Tamaki, K., Suyehiro, K., Allan, J., McWilliams, M., et al. [Eds], Proceedings of the Ocean Drilling Program, Scientific Results 127/128, Part 2, College Station, Texas: Ocean Drilling Program, pp. 819-836.

Kang, D.J., Kim, K., Kim, K.R., 2004. The past, present and future of the East/Japan Sea in change: a simple moving-boundary box model approach. Progress in Oceanography 61, 175–191.

Kim, H.J., Lee, G.H., Jou, H.T., Cho, H.M., Yoo, H.S., Park, G.T., Kim, J.S., 2007. Evolution of the eastern margin of Korea: constraints on the opening of the East Sea (Japan Sea). Tectonophysics 436, 37–55.

Kim, H.-J., Lee, G.H., Choi, D.-L., Jou, H.-T., Li, Z., Zheng, Y., Kim, G.-Y., Lee, S.-H., 2015. Back-arc rifting in the Korea Plateau in the East Sea (Japan Sea) and the separation of the southwestern Japan Arc from the Korean margin. Tectonophysics 638, 147–157. DOI: 10.1016/j.tecto.2014.11.003

Kim, G.B., Yoon, S.H., Sohn, Y.K., Kwon, Y.K., 2013. Wave-planation surfaces in the mid-western East Sea (Sea of Japan): Indicators of subsidence history and paleogeographic evolution of back-arc basin. Marine Geology 344, 65–81. DOI: 10.1016/j.margeo.2013.07.008

Kim, K., Kim, K.R., Kim, Y.G., Cho, Y.K., Chung, J.Y., Choi, B.H., Byun, S.K., Hong, G.H., Takematsu, M., Yoon, J.H., Volkov, Y., Danchenkov, M., 1996. New findings from CREAMS observations: water masses and eddies in the East Sea. Journal of Korean Society Oceanography 31, 155–163.

Klein, G. de V., 1985. The control of depositional depth, tectonic uplift and volcanism on sedimentation processes in the back-arc basins of the western Pacific Ocean. J. Geol. 93, 1–25.

Kwon, Y.K., Yoon, S.H., Chough, S.K., 2009. Seismic stratigraphy of the western South Korea Plateau, East Sea: implications for tectonic history and sequence development during back-arc evolution. Geo-Marine Letters 29(3), 181–189. DOI: 10.1007/s00367-009-0133-y

Lee, E., Kim, S., Nam, S., 2008. Paleo-Tsushima Water and its effect on surface water properties in the East Sea during the last glacial maximum: Revisited. Quaternary International 176-177, 3–12.

Lee, H.J., Chough, S.K., Yoon, S.H., 1996. Slope-stability change from late Pleistocene to Holocene in the Ulleung Basin, East Sea (Japan Sea). Sedimentary Geology 104, 39–51.

Lee, G.H, Kim, B., 2002. Infill history of the Ulleung Basin, East Sea (Sea of Japan) and implications on source rocks and hydrocarbons. Marine and Petroleum Geology 19, 829–845.

Lee, G.H., Yoon, Y.H., Nam, B., Lim, H., Kim, Y.-S., Kim, H.J., and Lee, K., 2011. Structural evolution of the southwestern margin of the Ulleung Basin, East Sea (Japan Sea) and tectonic implications. Tectonophysics 502, 293–307.

Lelikov, E.P., and Bersenev, I.I., 1975. Early Proterozoic Gness-migmatite complex of the Japan Sea, Southwestern part. Proc. Academic Sci. U.S.S.R., V. 223, pp. 676–679.

Marsaglia, K.M., 1995. Interarc and backarc basins. In C.J. Busby &R.V. Ingersoll, Tectonics of Sedimentary Basins. Pp. 299-329. Cambridge, Blackwell Science.

Marsaglia, K.M., Boggs Jr, S., Clift, P., Seyedolali, A., Smith, R. 1995. Sedimentation in western Pacific backarc basins: new insights from recent ODP drilling. In B. Taylor &J. Natland, Active Margins and Marginal Basins of the Western Pacific (pp. 292-314). American Geophysical Union Monograph Series 88.

Park, Y., Ree, J.H., Yoo, S.H., 2006. Fault slip analysis of Quaternary faults in southeastern Korea. Gondwana Research 9, 118−125.

Pisciotto, K.A., Ingle, J.C., Jr., von Breymann, M.T., Barron, J., et al., 1992. Proc. ODP Scientific Results 127/128 (Part 1) College Station, TX (Ocean Drilling Program). DOI: 10.2973/odp.pro.sr.127128-2.1992.

Rangin, C., Silver, E. A., von Breymann, M. T., et al., 1990. Proc. ODP, Init. Repts., 124: College Station, TX (Ocean Drilling Program).

Schellart, W., Jessell, M.W., Lister, G.S., 2003. Asymmetric deformation in the backarc region of the Kuril arc, northwest Pacific: New insights from analogue modeling. Tectonics 22 (5), 1047.

Seung, Y.H., Yoon, J.H., 1995. Robust diagnostic modeling of the Japan Sea circulation. Journal of Oceanography 51, 421–440.

Sdrolias, M. and Müller, R. D., 2006. Controls on back-arc basin formation. Geochem., Geophys., Geosyst. 7, Q04016.

Tada, R., 1994. Paleoceanographic evolution of the Japan Sea. Palaeogeogr., Palaeoclimatol., Palaeoecol. 108(3–4), 487–508. DOI: 10.1016/0031-0182(94)90248-8.

Tada, R., Irino, T., 1999. Land-ocean linkages over orbital and millennial timescales recorded in the late Quaternary sediments of the Japan Sea. Paleoceanography 14, 236–247.

Tada R., Murray R.W., Alvarez Zarikian, C.A., and Expedition 346 Scientists, 2015. Proceedings of the Integrated Ocean Drilling Program Volume 346, College Station, TX (Integrated Ocean Drilling Program). DOI: 10.2204/iodp.proc.346.2015.

Taira, A., 2001. Tectonic evolution of the Japanese Island arc system. Annu. Rev. Earth Planet. Sci. 29, 109–34. DOI: 10.1146/annurev.earth.29.1.109.

Tamaki, K., Suyehiro, K., Allan J., Ingle, J.C., Pisciotto, K., 1992. Tectonic synthesis and implications of Japan Sea ODP drilling, Proc. Ocean Drill. Program Sci. Results 127-128, 1333–1350.

Tamaki, K., 1988. Geological structure of the Japan Sea and its tectonic implications. Bull. Geol. Surv. Jpn. 39, 269–365.

Taylor, B., 1992. Rifting and the volcano-tectonic evolution of the Izu-Bonin-Mariana arc, in Taylor, B, Fujioka, K., Janecek, T., and Langmuir, C., eds., Proceedings of the Ocean Drilling Program, Scientific results, Volume 126, College Station, Texas, Ocean Drilling Program, p. 627–651.

Teague, W.J., Jacobs, G.A., Perkins, H.T., Book, J.W., Chang, K.I., Suk, M.S., 2002. Low frequency current observations in the Korea Strait. Journal of Physical Oceanography 32, 1621–1641.

Uyeda, S., 1991. The Japanese Island Arc and the subduction process. Episodes 14, 190–198.

Wright, I. C., 1997. Morphology and evolution of the remnant Colville and active Kermadec arc ridges south of 33° 30′ S. Mar. Geophys. Res. 19, 177–193.

Yoon, S.H., 1994. The Eastern Continental Margin of Korea: Stratigraphy, Geological Structure and Tectonic Evolution. Ph.D. Thesis, Seoul National Univ., 235 pp.

Figure Captions

Fig. 1: Physiographic map of the East Sea and the adjoining areas. The black rectangle outlines the area shown in Fig. 2A. Circles in pink, which were labeled with 01 and 02, indicate the locations of dredges samples over the SKP (Lelikov and Bersenev, 1975). *SKP*: South Korea Plateau, *NKP*: North Korea Plateau, *OB*: Oki Bank, *UB*: Ulleung Basin, *YB*: Yamato Basin, *YR*: Yamato Ridge, *JB*: Japan Basin, *KP*: Korea Gap (also known *UIG*: Ulleung Interplain Gap), *TWC*: Taiwan Warm Current, *TSS*: Tsushima Strait, *TGS*: Tsugaru Strait, *SS*: Soya Strait, *MS*: Mamiya Strait, *JB*: Japan Basin, *TB*: Tsushima/Ulleung Basin, *YB*: Yamato Basin, *YR*: Yamato Rise.

Fig. 2: (A) Study area and distribution of multi-channel seismic data (black lines) and the IODP drill site and previous gas hydrate drilling site locations. Heavy red lines with numbers indicate seismic profiles shown in other figures. *WSKP*: Western South Korea Plateau, *NUT*: North Ulleung Trough, *ESKP*: Eastern South Korea Plateau. Yellow lines denote bathymetric profiles shown in Fig. 2B. (B) Bathymetric profiles 1 and 2 illustrating the main structural features along the East Sea. The Ulleung Basin lies in water depth of 2,200 m. The Ulleung Island is a large seamount rising from abyssal depths of 2,100 m to a planated summit at about 100 m water depth. The WSKP is separated from the ESKP by the North Ulleung Trough (NUT).

Fig. 3: Seismic profile crossing IODP Expedition 346 Site U1430 on the ESKP in E-W direction. Seismic-to-well tie is illustrated by synthetic correlation (Table 1) using acoustic (VCO) and density (RHO) logs at Hole U1430B. The megasequence boundaries in the study area are assigned with geological ages with the help of the seismic-to-well tie. Lithologies and lithologic unit boundaries were taken from Tada et al. (2015). Lines in blue are NGR and

GRA (gamma ray attenuation) density logs taken from sediment cores by WR-MSCL (whole round multi-sensor core logger) in full coverage.

Fig. 4: (a) Seismic profile crossing the ESKP and the UIG in E-W direction. (b) Interpretation of (a). MB1 is disrupted by basement-bounding faults at various scales giving rise to buried sub-basins between faulted bocks. Locally, the basement highs show flat top surfaces. The uppermost seismic section of the UIG, which is below the arrow representing bottom currents, appears to have undergone recent, significant erosion at the seafloor. See Fig. 2 for location.

Fig. 5: (a) Seismic profile crossing the ESKP and the UIG in N-S direction. (b) Interpretation of (a). The interpreted section exhibits major structural features of the area and all the unconformities or megasequence boundaries as well as the megasequences. MS1 is confined in the basement grabens and shows wedge-shape geometries. MB1 is cut by normal faults. MS2 completely covers the underlying horst and graben topography. The box indicates the zoom shown in Fig. 8. See Fig. 2 for location.

Fig. 6: (a) Seismic profile crossing the ESKP and the UIG in N-S direction. (b) Interpretation of (a). The top of the acoustic basement (MB1) is cut by numerous faults. MB2 forms a prominent unconformity and terminates against shallow basement highs. MS1 appears to be abundantly faulted and folded and most of the secondary faults die out immediately below MS2. MS3 is composed of undeformed sheet-drape sediments. The box indicates the zoomed area shown in Fig. 9. See Fig. 2 for location.

Fig. 7: (a) Seismic profile traversing the ESKP and the UIG in E-W direction. (b) Interpretation of (a). MB1 is offset by numerous faults and MS1 appears to be intensely deformed. MB2 and MB3 terminate against basement highs. The seismic profile also exhibits seafloor erosion at the base of plateau along the UIG. The box denotes the enlarged section shown in Fig. 10. See Fig. 2 for location.

Fig. 8: (a) Zoom of a part of the N-S trending seismic profile displayed in Fig. 5. (b) Interpretation of (a). MS1 clearly shows a wedge-shaped sedimentary infill along the half-graben structure, indicating syn-depositional faulting. (c) Close-up of (b) on the northern half-graben of the plateau. MB2 is characterized by erosional truncation over the basement high; here, the sediments below MB2 appear to have been tilted and leveled by that surface. See Fig. 2 for location.

Fig. 9: (a) Zoom of a part of the seismic profile displayed in Fig. 6. (b) Interpretation of (a). MS1 is characterized by discontinuous reflections with variable amplitude; this megasequence is significantly deformed by compressive structures including faults and folds. MS2 is characterized by low amplitude continuous reflections and fills the lower areas of MS1. (c) Close-up of (b) on the southern flank of a dipping graben. Locally, the uppermost layers of MS2 show tilting and truncation those are indicative of uplift and subsequent erosion. Truncation of sedimentary layers of MS2 towards the steep flanks of the plateau is also highlighted. MS3 includes continuous reflections of variable amplitude. A seafloor morphological step might represent a submarine landslide scar. See Fig. 2 for location.

Fig. 10: (a) Zoom of a part of the seismic profile displayed in Fig. 7. (b) Interpretation of (a). MS1 is characterized by low-to-high amplitude discontinuous reflections. It is also cut by numerous faults most of which die immediately below MB2. This may suggest reduced tectonic activity following the period of MS2 deposition. MS2 onlaps onto shallow basement highs and consists of low amplitude continuous reflections. MS3 is characterized by discontinuous reflections with variable amplitudes. See Fig. 2 for location.

Fig. 11: (a-c) Depth structure maps of megasequence boundaries. (a) MB1 (the top of the acoustic basement). MB1 is shallowest in the ESKP; the depths range from less than 1,000 m to over 4,000 m. The depth structure map further reveals that MB1 is cut by numerous NE-SW trending normal faults. (b) Depth structure map of MB2. The depths of the MB2 range

from less than 1,300 in the northwest to over 2,300 m in the southeast. (c) Depth structure map of MB3. MB3 deepens southeast from about 1,000 m to over 1,900 m.

Fig. 12: (a-c) Isopach maps of megasequences and (d) total thickness map. (a) MS1 (Late Oligocene and Late Middle Miocene). MS1 largely fills the basement grabens and half-grabens; its thickness ranges from less than 100 m to over 700 m. (b) MS2 (Late Middle Miocene and Latest Late Miocene). The thickness of MS2 ranges from about 100 over the basement highs to more than 350 m in the basement lows. (c) MS3 (Pliocene and Present). MS3 generally has a uniform thickness over the ESKP (average: 50 m); it is thickest (> 250 m) in the southeastern part of the Plateau. (d) Total thickness map. The total sediment thicknesses range from about 200 m to more than 1,000 m in the ESKP. The thickest sediments (> 2,400 m) occur in the northeastern part of the UIG.

Fig. 13: Crystalline mineral counts (per second) of quartz, plagioclase, and illite from XRD analysis of smear slides versus depth show distinct changes at the megasequence transitions from MS3 to MS1. Unit MS3 has higher quartz and feldspar contents than sediments in Unit MS2 which means a coarser (silty) terrigenous input in Unit MS3. Similarly, Unit MS3 has more abundant clay minerals compared to Unit MS2, which could be due at least in part to alteration of tephra layers deposited after MB2. Unit MS1 generally has a higher feldspar content than Unit MS2, which could reflect changes in sedimentary input from terrigenous to biogenic during the Miocene.

Fig. 14: Mineral composition diagrams of quartz versus plagioclase (A), quartz versus kaolinite+chlorite (B), smectite versus illite (C), plagioclase versus k-feldspar counts (D). Unit MS3 sediments show the highest plagioclase content, i.e., (A) and (D), and plagioclase content in the MS3 unit is higher than MS2. Higher plagioclase content at a given quartz content (A) in the Unit MS1 (i.e., lower quartz/feldspar ratio) support a more immature composition of the coarse terrigenous component in this unit compared to the other two units

recovered at Site U1430. Clay minerals, shown in (B) and (C), are the highest in content within the sediments of MS1, while clay content of MS3 is higher than MS2.

Fig. 15: Schematic illustration of the geological evolution of the ESKP. (a) Stage 1 was characterized by rifting and extension that led to the formation of several basement ridges and troughs bound by normal faults. Shallow-water conditions prevailed. The syn-rift units show divergent reflections, suggesting synchronous deposition and faulting. Moderate- to- high-amplitude, discontinuous reflections suggest non-marine sedimentation, mainly of fluvial-lacustrine nature, whereas horst flat tops suggest erosion. Extension and subsidence were punctuated by uplift in the latest Middle Miocene (ca. 13 Ma) as identified by folding of MS1 sediments at some locations. MB2 appear as an erosional unconformity indicating tilting of fault blocks and subsequent erosion. (b) Stage 2 was a phase of relative tectonic quiescence along the ESKP, when marine conditions were established over the plateau. Thick marine sediments of hemipelagic origin infilled the grabens and half grabens and draped the basement highs. The end of Stage 2 was marked by a major unconformity that indicated a long hiatus (ca. 7 Ma – 4.5 Ma). (c) Stage 3 has been characterized by lowered subsidence rates and dominance of hemipelagic sedimentation. Bottom currents have been active at the base of the outer margin of the plateau where it meets the UIG.

Table captions

Table 1. Correlation between synthetic seismogram and seismic traces at Hole U1430B which is over 80%.

Table 2. Geological evolution of the ESKP since the Oligocene shown with regional movements in response to plate motions and tectonic events, and eustatic changes. Seafloor spreading initiated rifting at ca. 28 Ma and it is followed by subsidence until the arrival of the

Philippine Sea Plate under SW Japan which caused uplift and erosion in the ESKP. Shallow-marine conditions prevailed at this period when the global sea-level trend was high. Post-rift stage between ca. 11.8–7 Ma is composed of regional subsidence with a shift to marine environment which is also coherent to global sea-level rise. A short-lived tectonic uplift due to Eastern movement of Amur Plate caused inversion in the southern margin of the East Sea and the western WSKP, and locally in the eastern part of the ESKP. The recent post-rift stage since 4.5 Ma consists of regional subsidence with pelagic sedimentation in the ESKP, while the global sea-level was overall lowering. Eustatic curves are from Haq et al. (1987) and ages are from Berggren et al. (1995).

Figures

Fig. 1

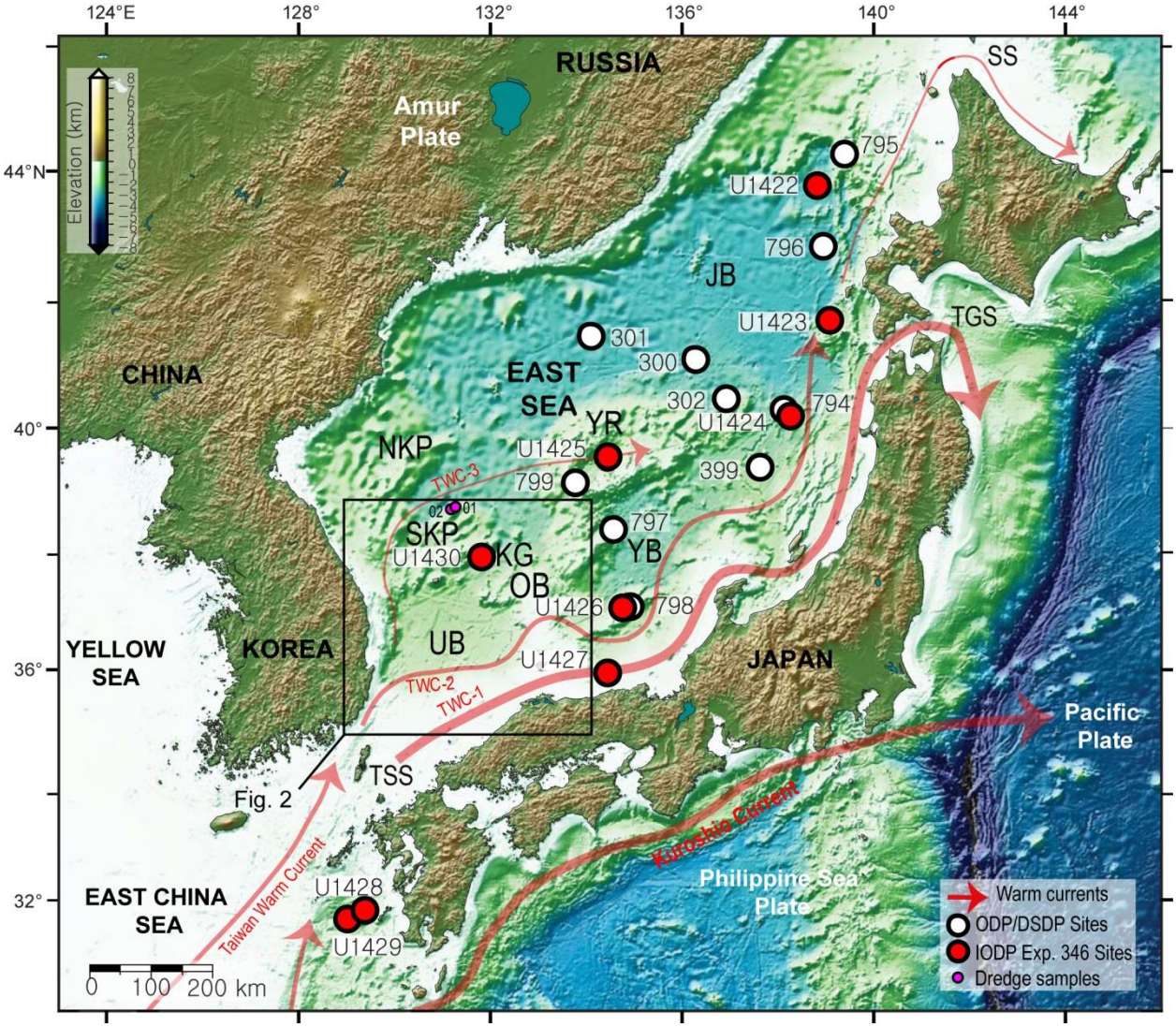

Fig. 2

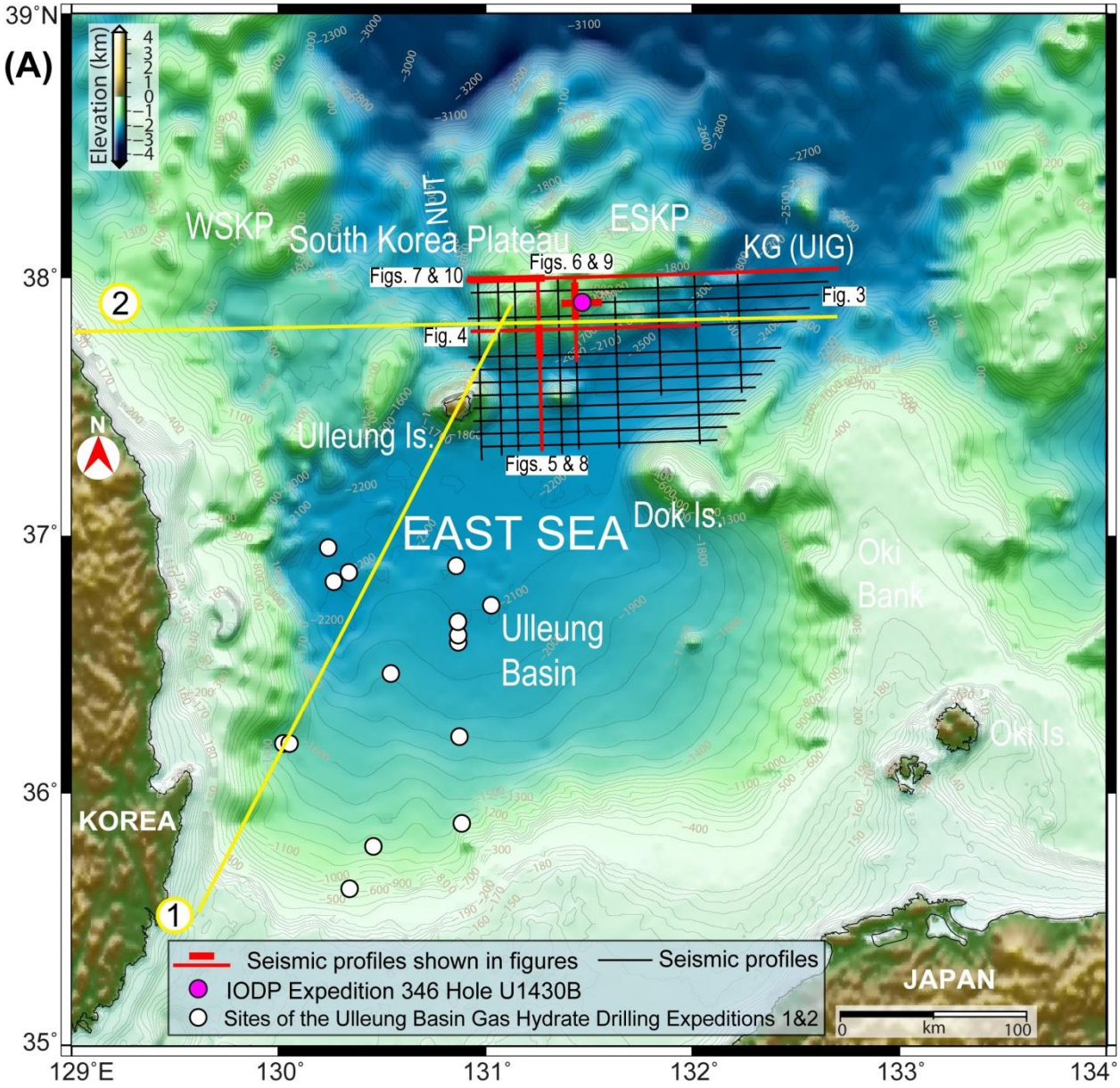
(A)
39°N
38°
37°
36°
35°
129°E
130°
131°
132°
133°
134°
Elevation (km)
WSKP
South Korea Plateau
NUT
ESKP
KG (UIG)
Figs. 7 & 10
Figs. 6 & 9
Fig. 3
Fig. 4
Figs. 5 & 8
Ulleung Is.
EAST SEA
Dok Is.
Oki Bank
Ulleung Basin
Oki Is.
KOREA
JAPAN
N
1
2
Seismic profiles shown in figures
Seismic profiles
IODP Expedition 346 Hole U1430B
Sites of the Ulleung Basin Gas Hydrate Drilling Expeditions 1&2
0
km
100

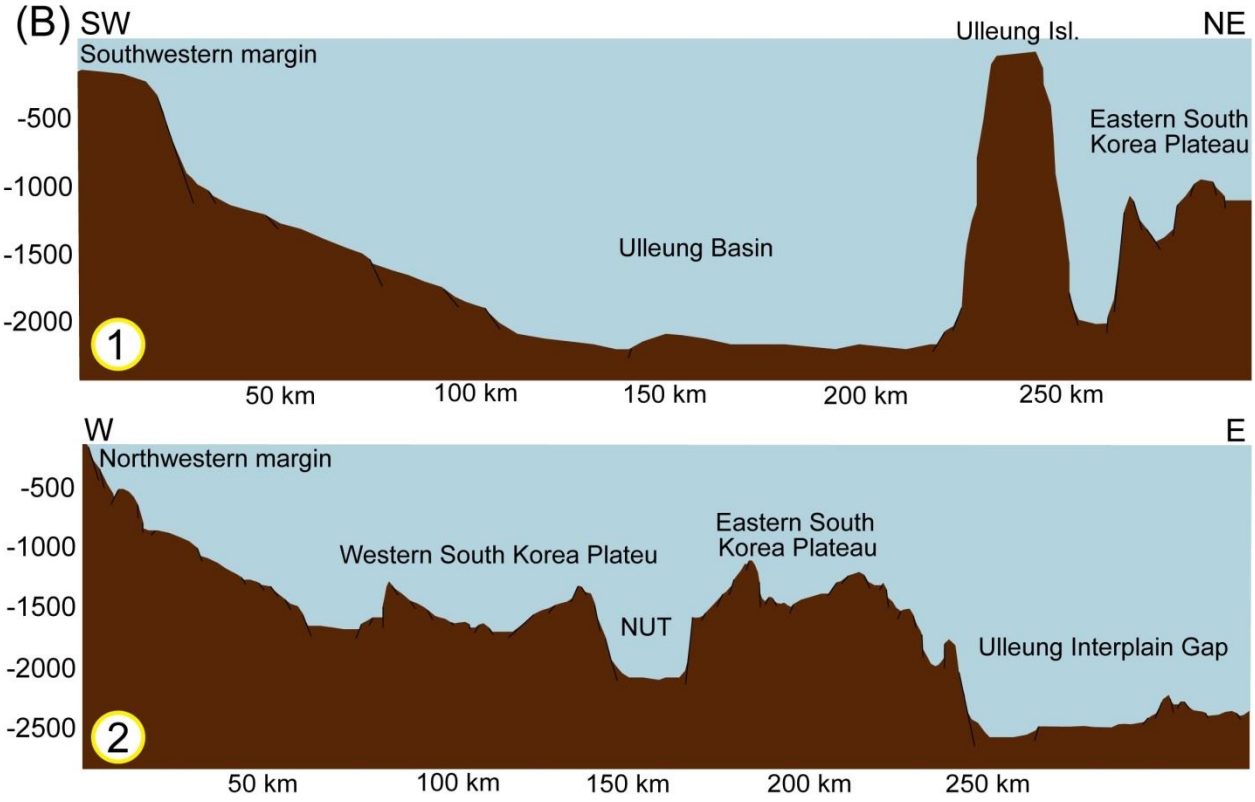
(B) SW
Southwestern margin
Ulleung Isl.
NE
-500
-1000
-1500
-2000
Eastern South
Korea Plateau
Ulleung Basin
1
50 km
100 km
150 km
200 km
250 km
W
E
Northwestern margin
-500
-1000
-1500
-2000
-2500
Western South Korea Plateu
Eastern South
Korea Plateau
NUT
Ulleung Interplain Gap
2
50 km
100 km
150 km
200 km
250 km

Fig. 3

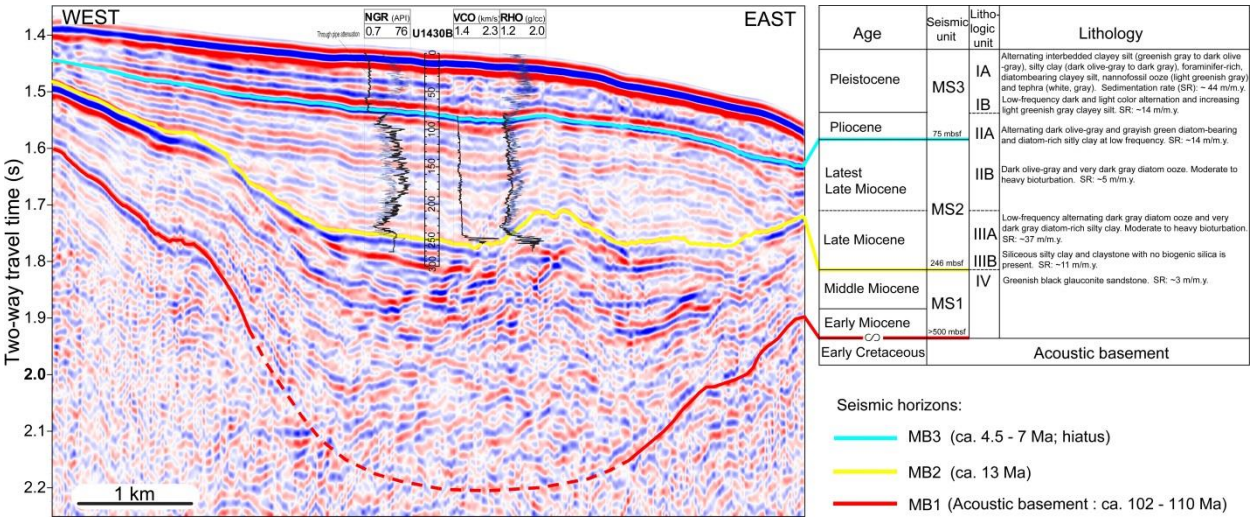
WEST
EAST
NGR (API)
0.7 76
U1430B
VCO (km/s) RHO (g/cc)
1.4 2.3 1.2 2.0
Two-way travel time (s)
1.4
1.5
1.6
1.7
1.8
1.9
2.0
2.1
2.2
1 km
Age
Seismic unit
Litho-logic unit
Lithology
Pleistocene
MS3
IA
Alternating interbedded clayey silt (greenish gray to dark olive -gray), silty clay (dark olive-gray to dark gray), foraminifer-rich, diatombearing clayey silt, nannofossil ooze (light greenish gray) and tephra (white, gray). Sedimentation rate (SR): ~ 44 m/m.y.
IB
Low-frequency dark and light color alternation and increasing light greenish gray clayey silt. SR: ~14 m/m.y.
Pliocene
75 mbsf
IIA
Alternating dark olive-gray and grayish green diatom-bearing and diatom-rich silty clay at low frequency. SR: ~14 m/m.y.
Latest Late Miocene
IIB
Dark olive-gray and very dark gray diatom ooze. Moderate to heavy bioturbation. SR: ~5 m/m.y.
MS2
Late Miocene
IIIA
Low-frequency alternating dark gray diatom ooze and very dark gray diatom-rich silty clay. Moderate to heavy bioturbation. SR: ~37 m/m.y.
246 mbsf
IIIB
Siliceous silty clay and claystone with no biogenic silica is present. SR: ~11 m/m.y.
Middle Miocene
MS1
IV
Greenish black glauconite sandstone. SR: ~3 m/m.y.
Early Miocene
>500 mbsf
Early Cretaceous
Acoustic basement
Seismic horizons:
MB3 (ca. 4.5 - 7 Ma; hiatus)
MB2 (ca. 13 Ma)
MB1 (Acoustic basement : ca. 102 - 110 Ma)

Fig. 4

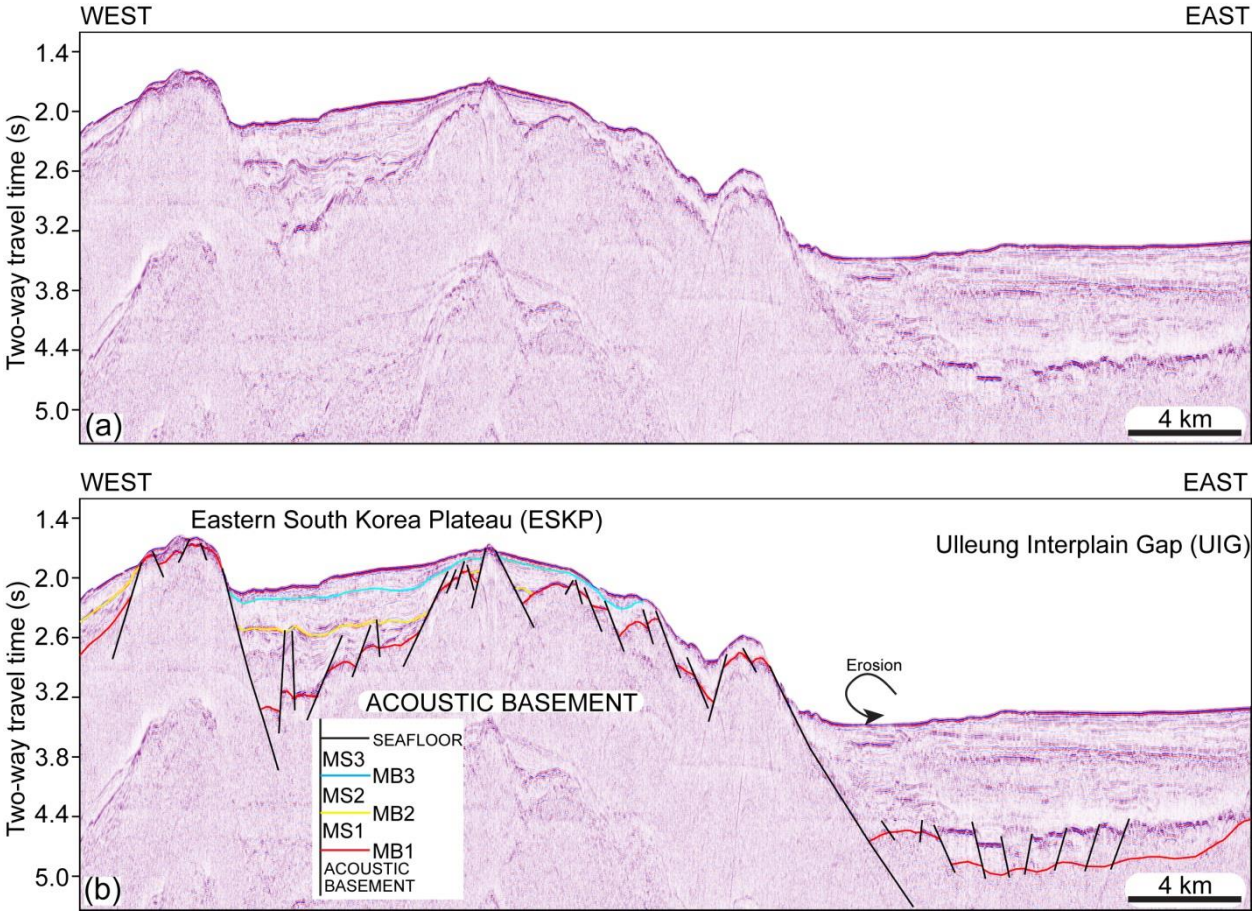
WEST
EAST
Two-way travel time (s)
1.4
2.0
2.6
3.2
3.8
4.4
5.0
(a)
4 km
WEST
EAST
Eastern South Korea Plateau (ESKP)
Ulleung Interplain Gap (UIG)
Erosion
ACOUSTIC BASEMENT
SEAFLOOR
MS3
MB3
MS2
MB2
MS1
MB1
ACOUSTIC BASEMENT
(b)
4 km

Fig. 5

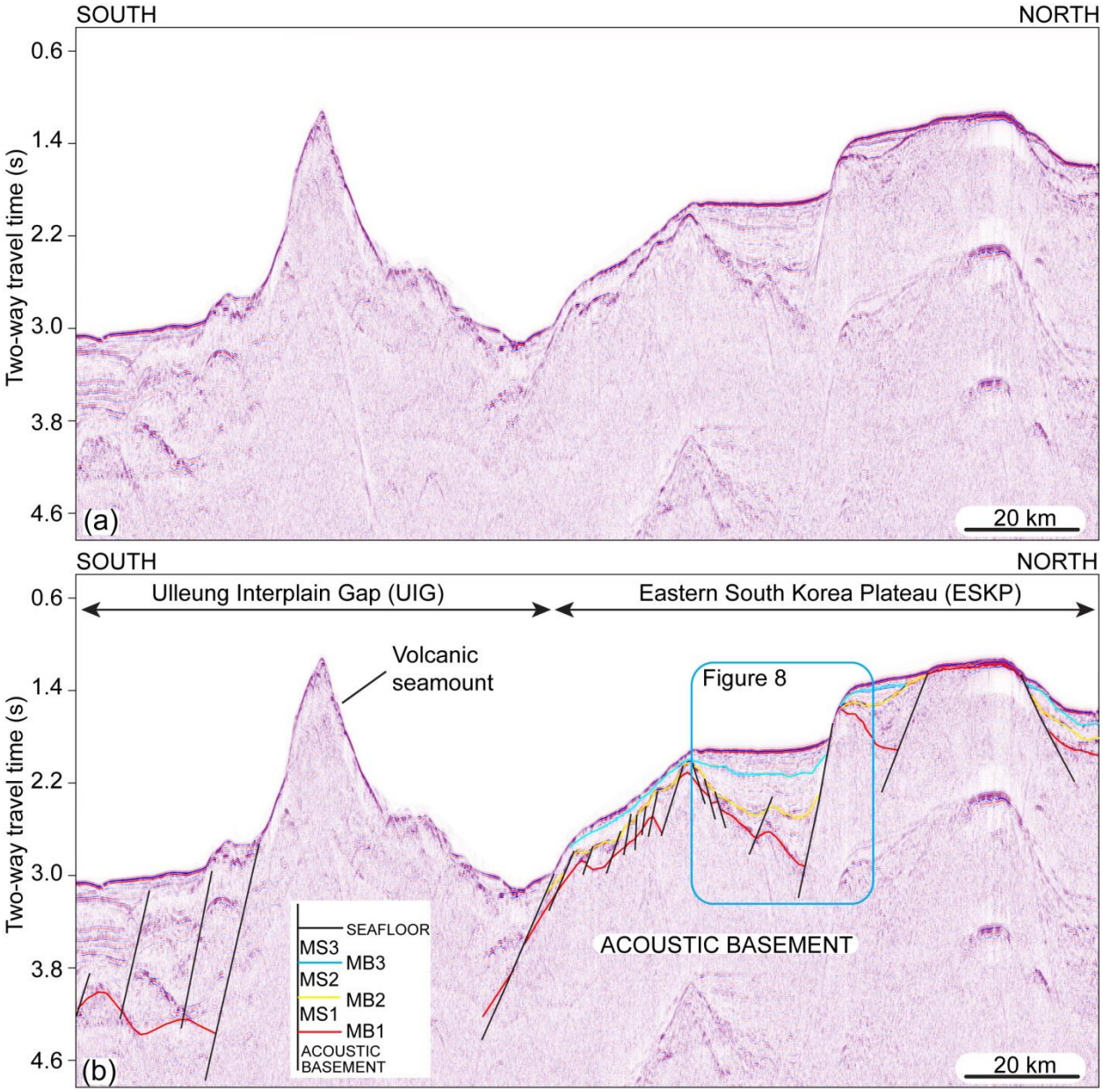
SOUTH
NORTH
Two-way travel time (s)
0.6
1.4
2.2
3.0
3.8
4.6
(a)
20 km
SOUTH
NORTH
Ulleung Interplain Gap (UIG)
Eastern South Korea Plateau (ESKP)
Volcanic seamount
Figure 8
SEAFLOOR
MS3
MB3
MS2
MB2
MS1
MB1
ACOUSTIC BASEMENT
ACOUSTIC BASEMENT
(b)
20 km

Fig. 6

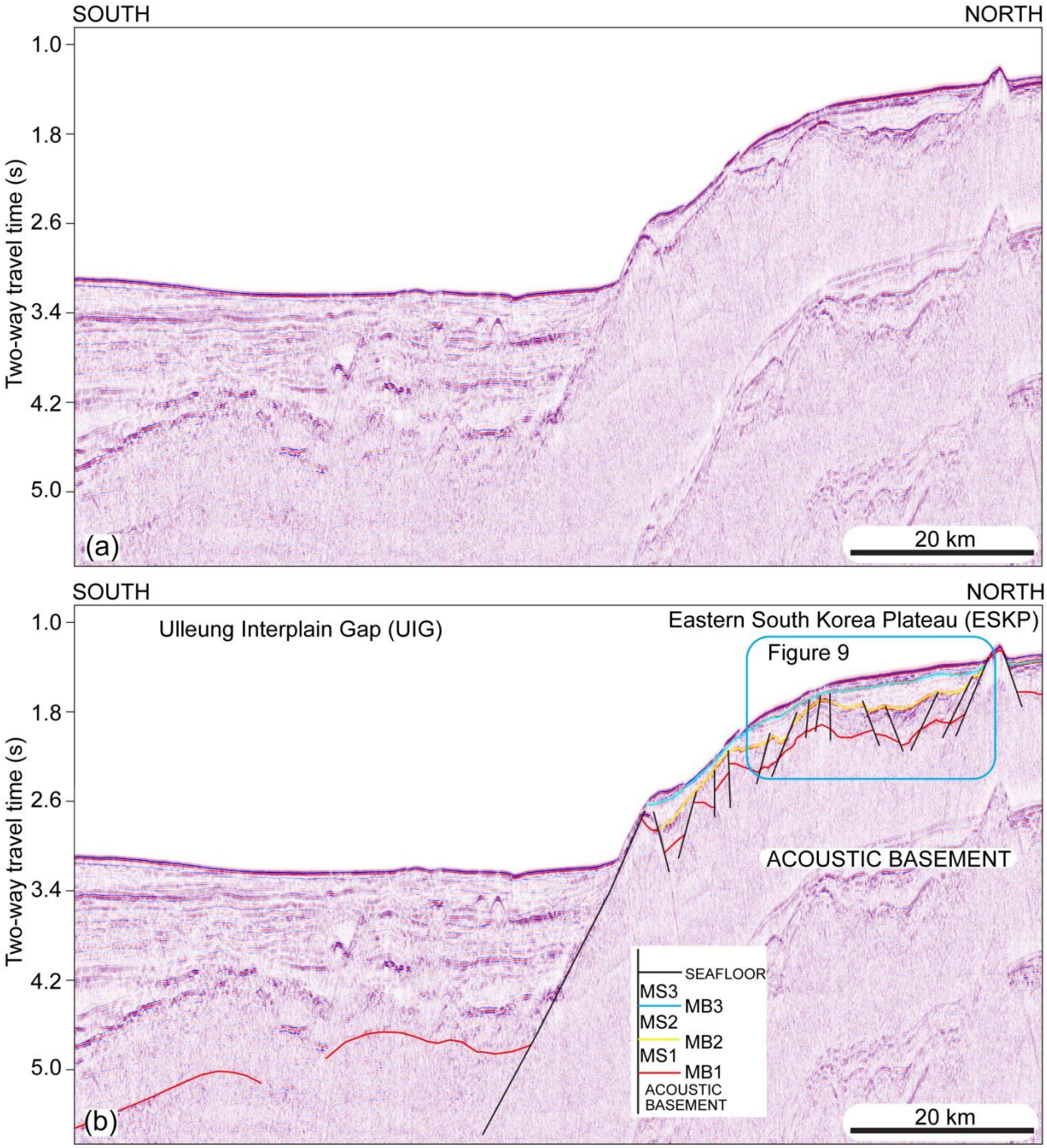
SOUTH
NORTH
1.0
1.8
2.6
3.4
4.2
5.0
Two-way travel time (s)
(a)
20 km
SOUTH
NORTH
Ulleung Interplain Gap (UIG)
Eastern South Korea Plateau (ESKP)
Figure 9
ACOUSTIC BASEMENT
SEAFLOOR
MS3
MB3
MS2
MB2
MS1
MB1
ACOUSTIC BASEMENT
(b)
20 km

Fig. 7

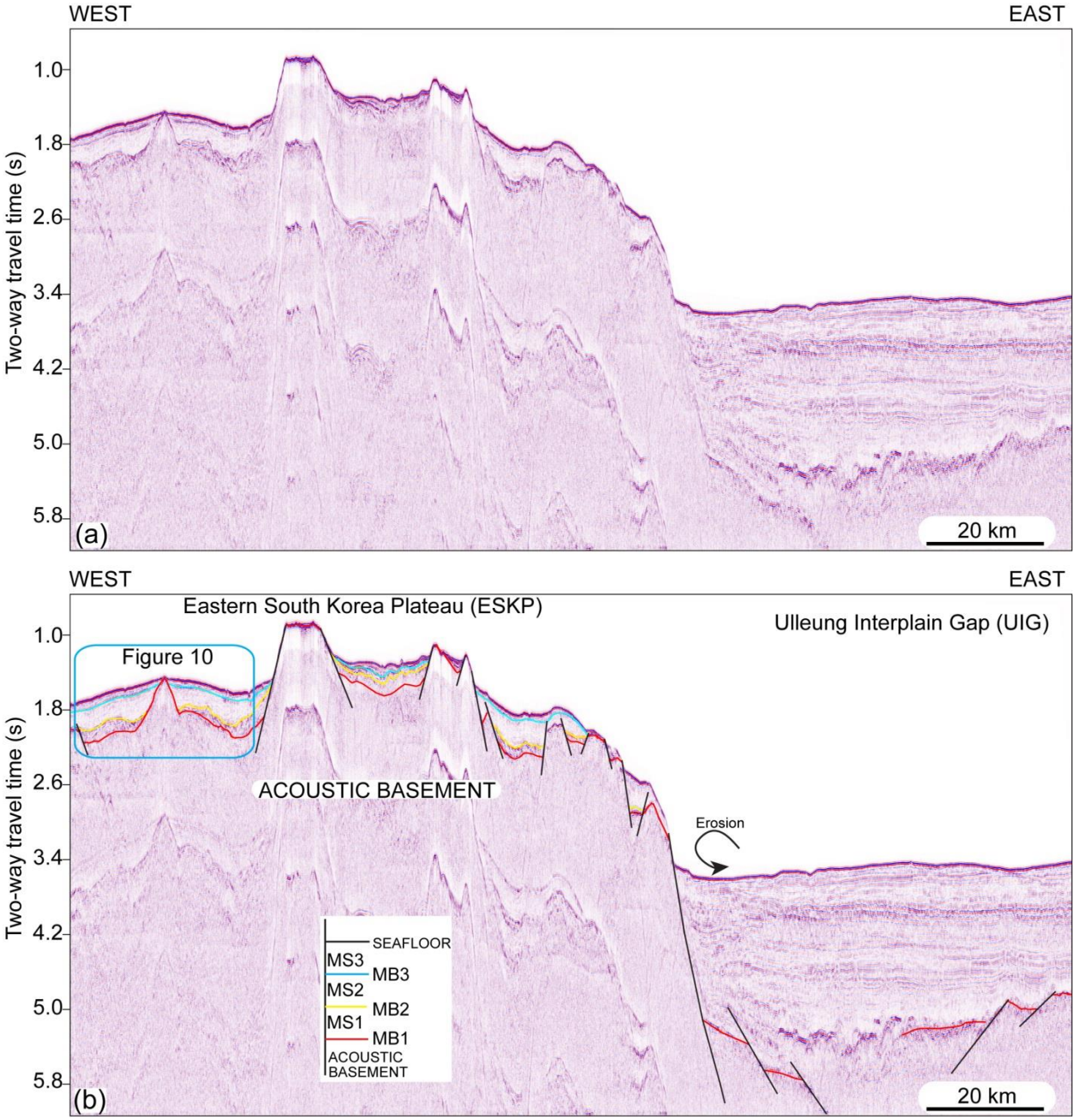
WEST
EAST
Two-way travel time (s)
1.0
1.8
2.6
3.4
4.2
5.0
5.8
(a)
20 km
WEST
EAST
Eastern South Korea Plateau (ESKP)
Ulleung Interplain Gap (UIG)
Figure 10
ACOUSTIC BASEMENT
Erosion
SEAFLOOR
MS3
MB3
MS2
MB2
MS1
MB1
ACOUSTIC BASEMENT
(b)
20 km

Fig. 8

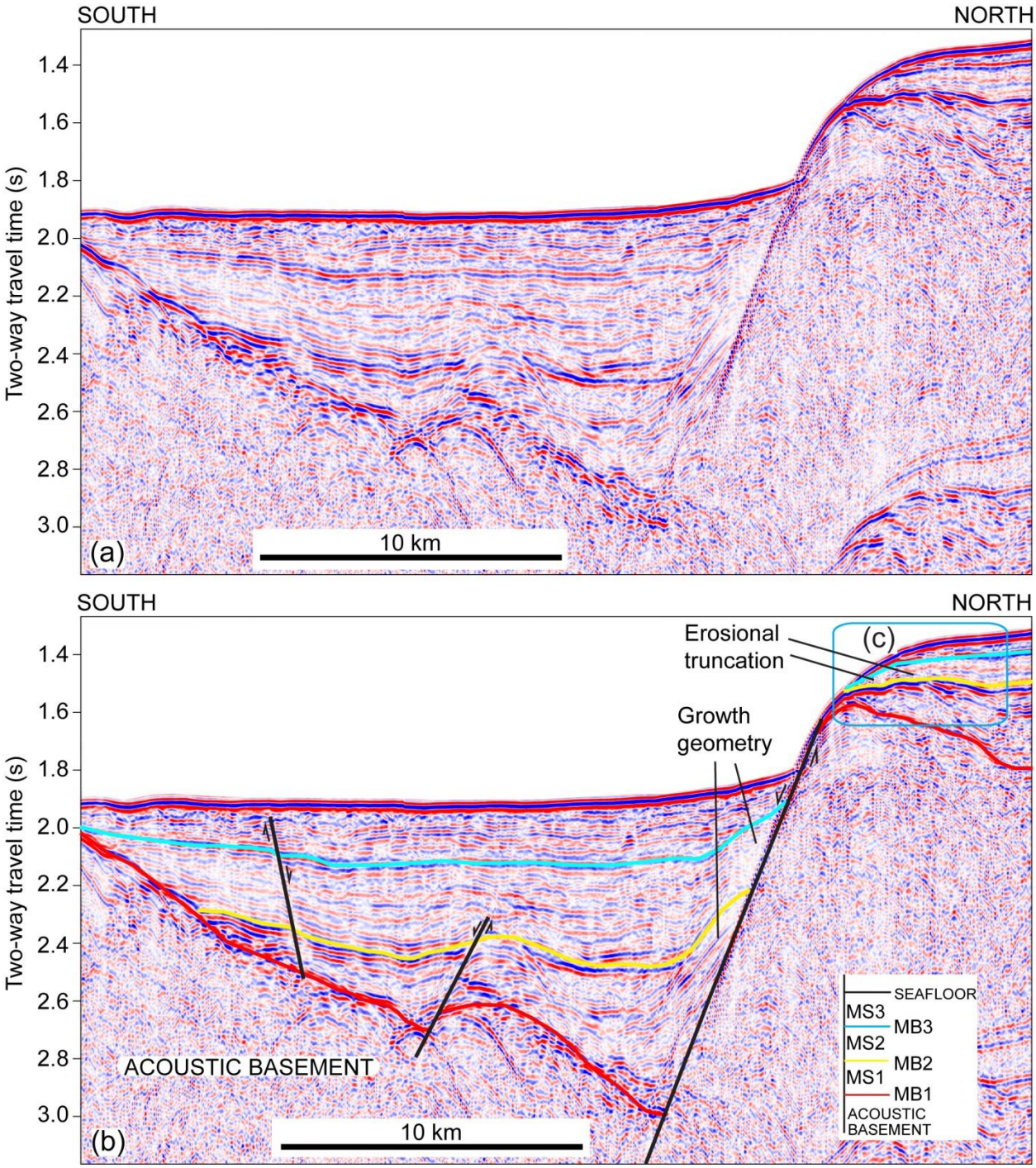
SOUTH
NORTH
Two-way travel time (s)
1.4
1.6
1.8
2.0
2.2
2.4
2.6
2.8
3.0
(a)
10 km
SOUTH
NORTH
Erosional truncation
(c)
Growth geometry
ACOUSTIC BASEMENT
(b)
10 km
SEAFLOOR
MS3
MB3
MS2
MB2
MS1
MB1
ACOUSTIC BASEMENT

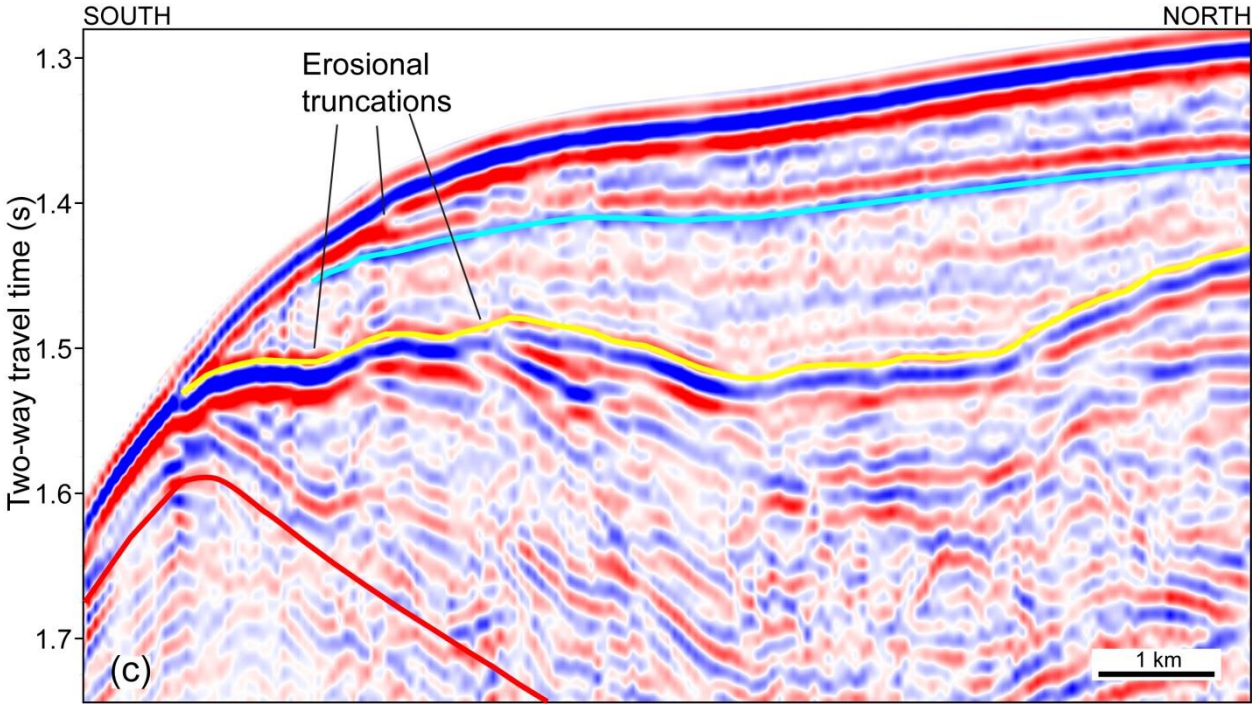
SOUTH
NORTH
Erosional
truncations
Two-way travel time (s)
1.3
1.4
1.5
1.6
1.7
(c)
1 km

Fig. 9

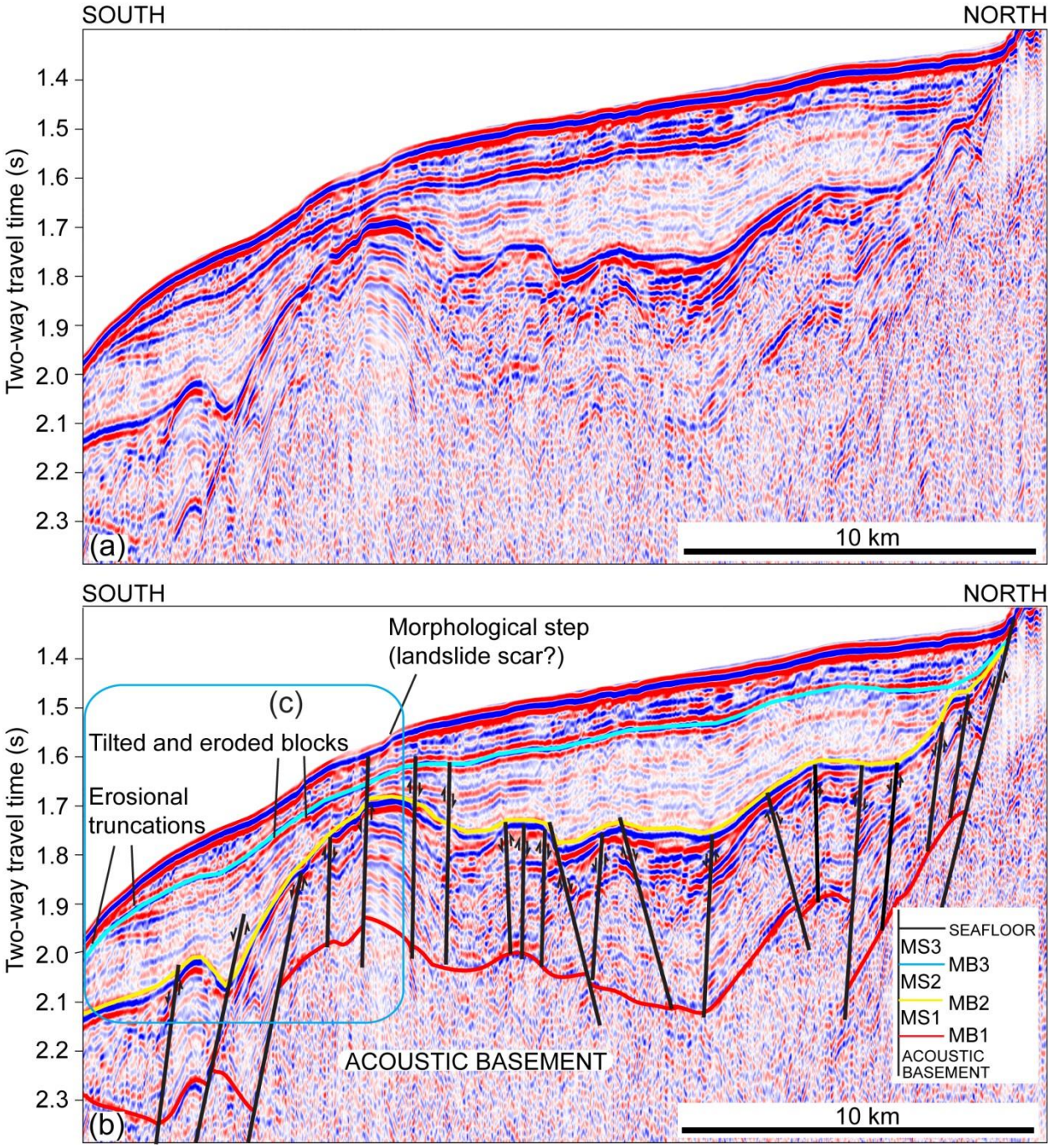
SOUTH
NORTH
Two-way travel time (s)
1.4
1.5
1.6
1.7
1.8
1.9
2.0
2.1
2.2
2.3
(a)
10 km
SOUTH
NORTH
Morphological step
(landslide scar?)
(c)
Tilted and eroded blocks
Erosional
truncations
ACOUSTIC BASEMENT
SEAFLOOR
MS3
MB3
MS2
MB2
MS1
MB1
ACOUSTIC
BASEMENT
(b)
10 km

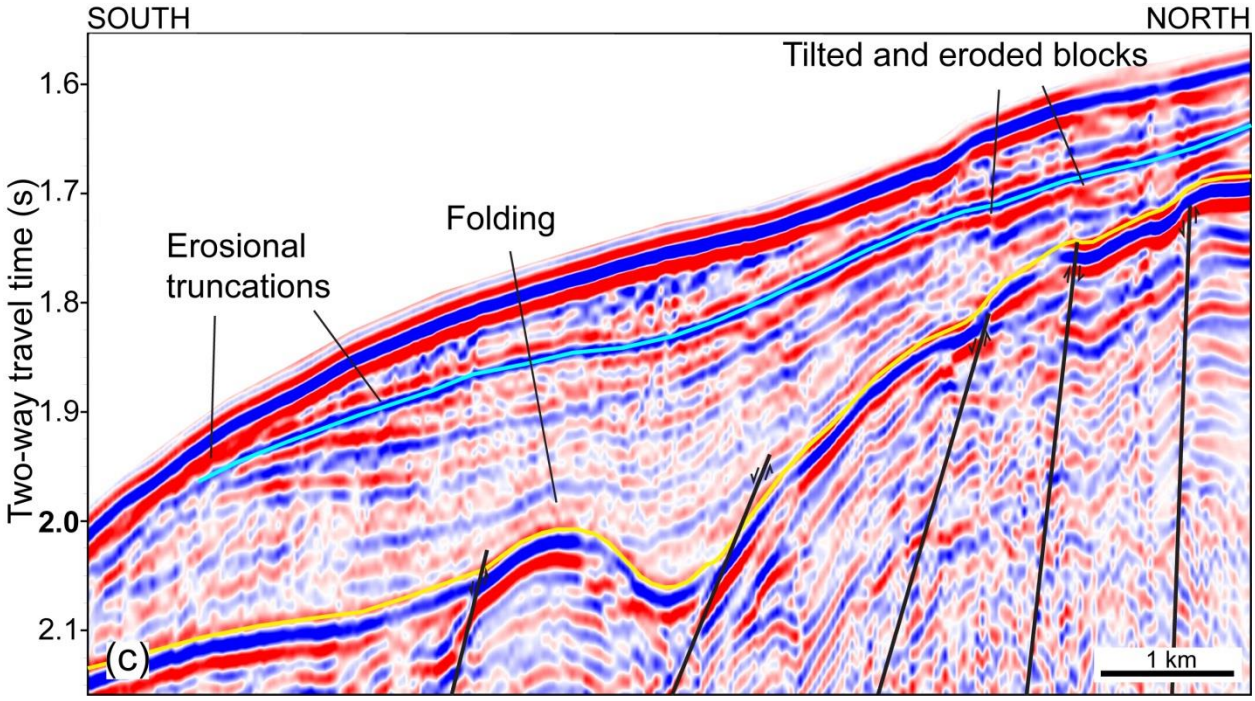
SOUTH
NORTH
Tilted and eroded blocks
Folding
Erosional
truncations
Two-way travel time (s)
1.6
1.7
1.8
1.9
2.0
2.1
(c)
1 km

Fig. 10

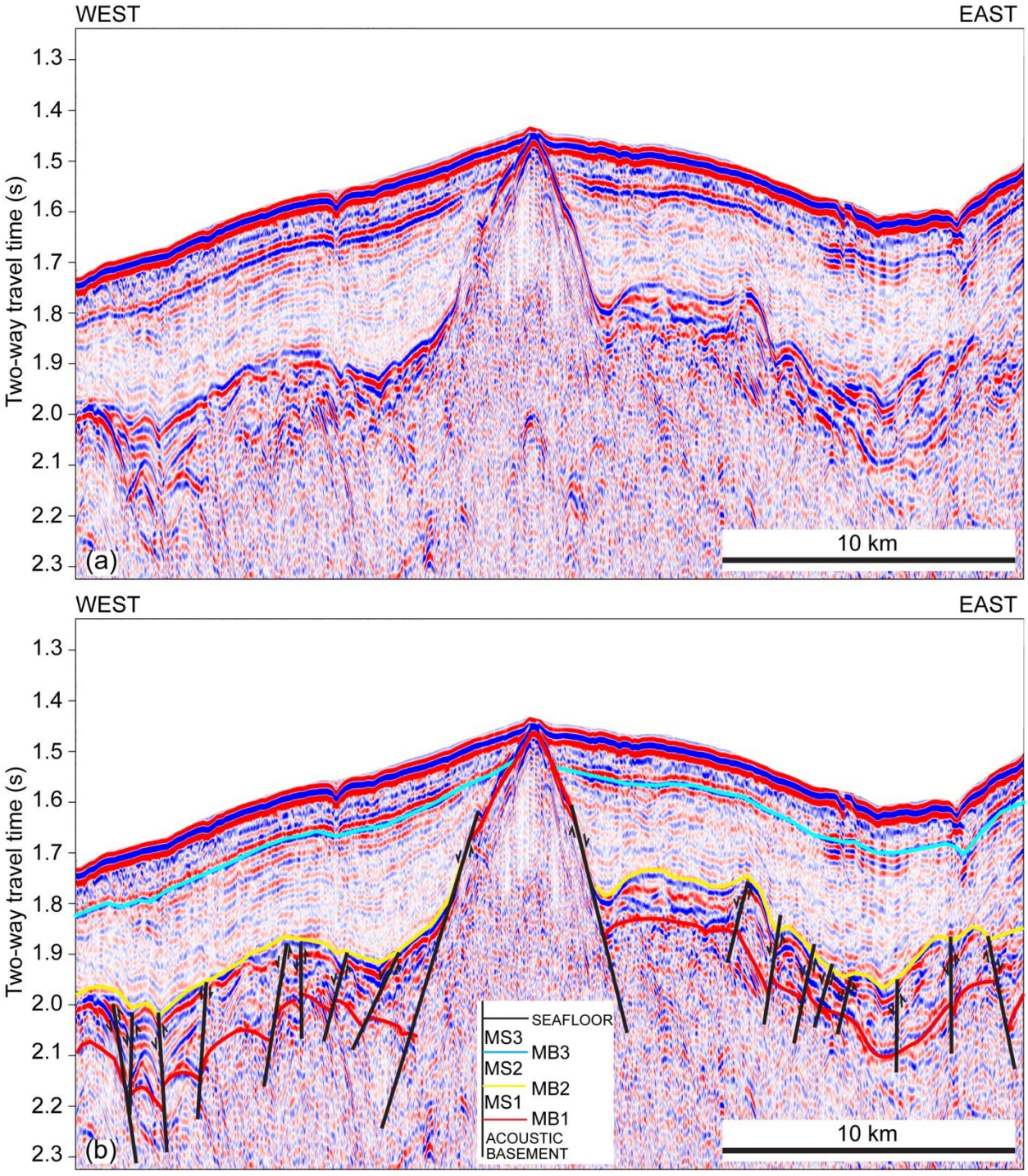
WEST
EAST
Two-way travel time (s)
1.3
1.4
1.5
1.6
1.7
1.8
1.9
2.0
2.1
2.2
2.3
(a)
10 km
WEST
EAST
Two-way travel time (s)
(b)
SEAFLOOR
MS3
MB3
MS2
MB2
MS1
MB1
ACOUSTIC BASEMENT
10 km

Fig. 11

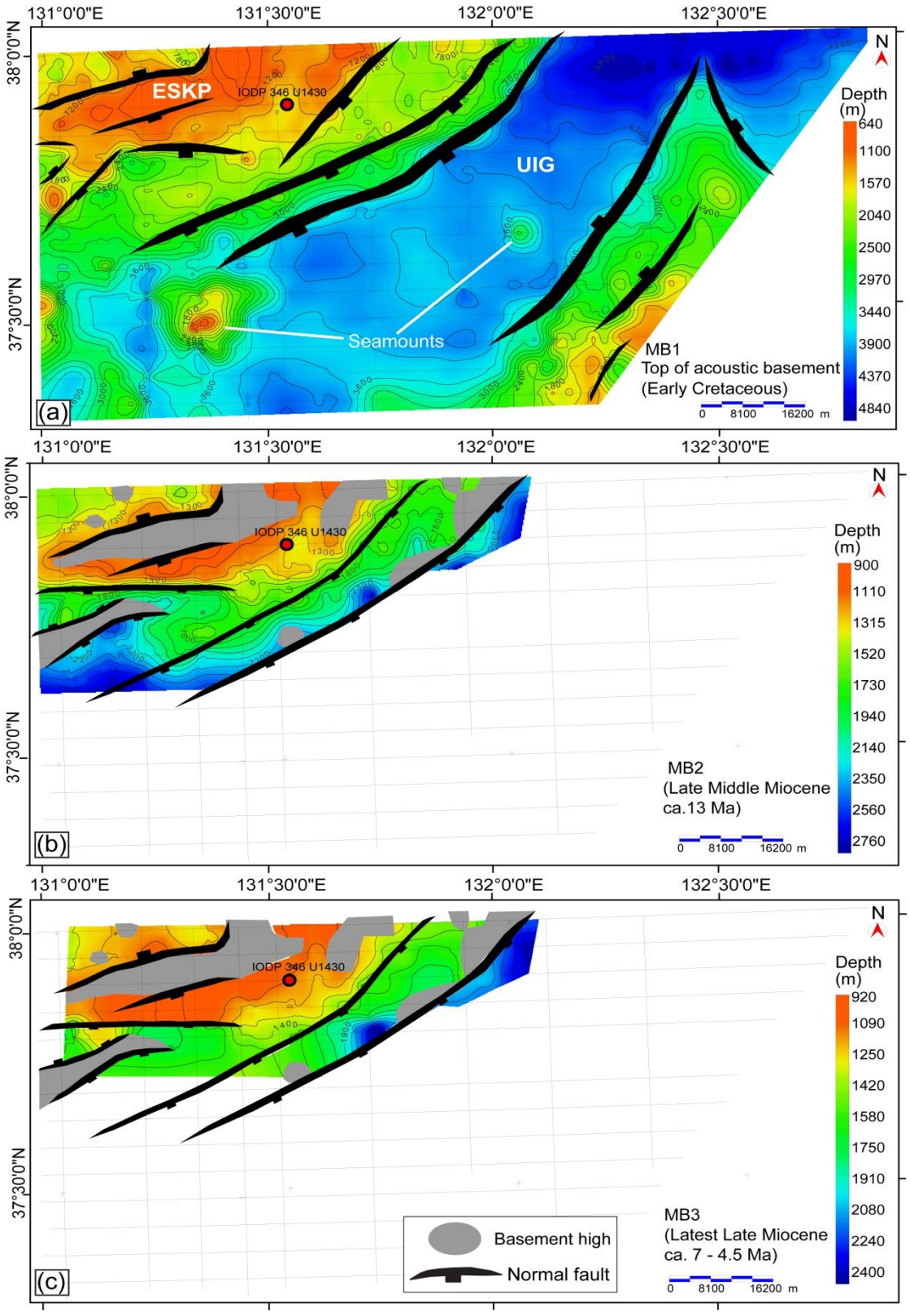
131°0'0"E
131°30'0"E
132°0'0"E
132°30'0"E
38°0'0"N
37°30'0"N
N
ESKP
IODP 346 U1430
UIG
Seamounts
Depth (m)
640
1100
1570
2040
2500
2970
3440
3900
4370
4840
MB1
Top of acoustic basement
(Early Cretaceous)
0 8100 16200 m
(a)
IODP 346 U1430
Depth (m)
900
1110
1315
1520
1730
1940
2140
2350
2560
2760
MB2
(Late Middle Miocene
ca.13 Ma)
0 8100 16200 m
(b)
IODP 346 U1430
Depth (m)
920
1090
1250
1420
1580
1750
1910
2080
2240
2400
Basement high
Normal fault
MB3
(Latest Late Miocene
ca. 7 - 4.5 Ma)
0 8100 16200 m
(c)

Fig. 12

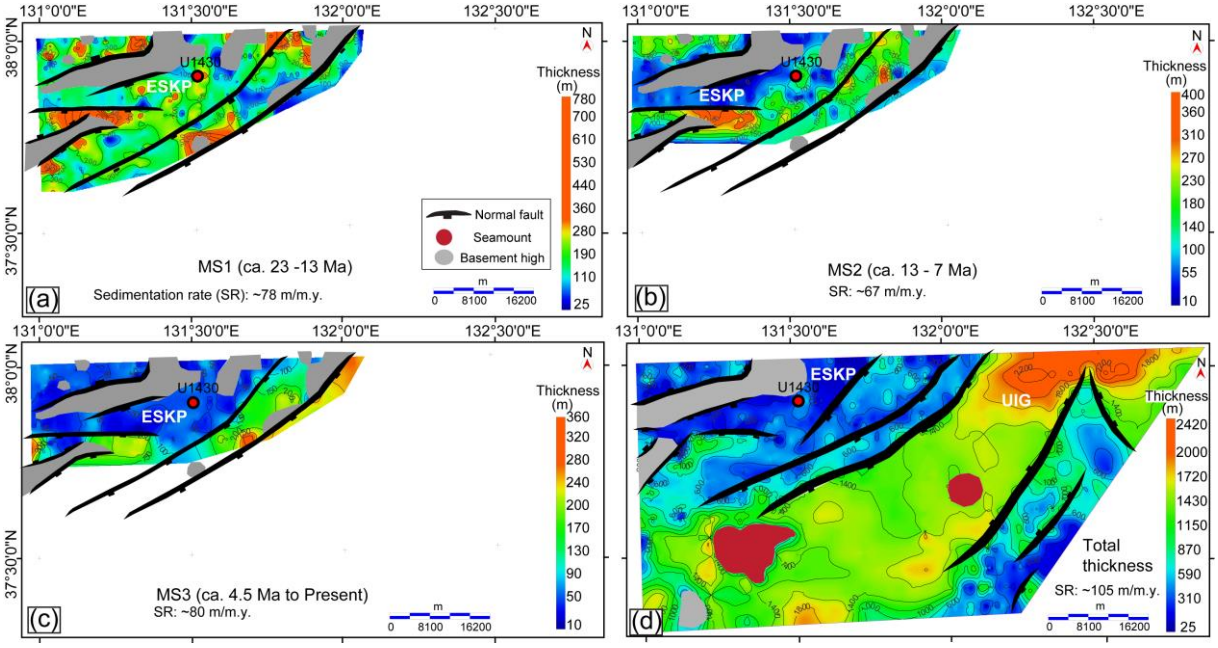
131°0'0"E
131°30'0"E
132°0'0"E
132°30'0"E
38°0'0"N
37°30'0"N
N
U1430
ESKP
UIG
Thickness (m)
780
700
610
530
440
360
280
190
110
25
400
360
310
270
230
180
140
100
55
10
360
320
280
240
200
170
130
90
50
10
2420
2000
1720
1430
1150
870
590
310
25
Normal fault
Seamount
Basement high
MS1 (ca. 23 -13 Ma)
Sedimentation rate (SR): ~78 m/m.y.
MS2 (ca. 13 - 7 Ma)
SR: ~67 m/m.y.
MS3 (ca. 4.5 Ma to Present)
SR: ~80 m/m.y.
Total thickness
SR: ~105 m/m.y.
m
0
8100
16200
(a)
(b)
(c)
(d)

Fig. 13

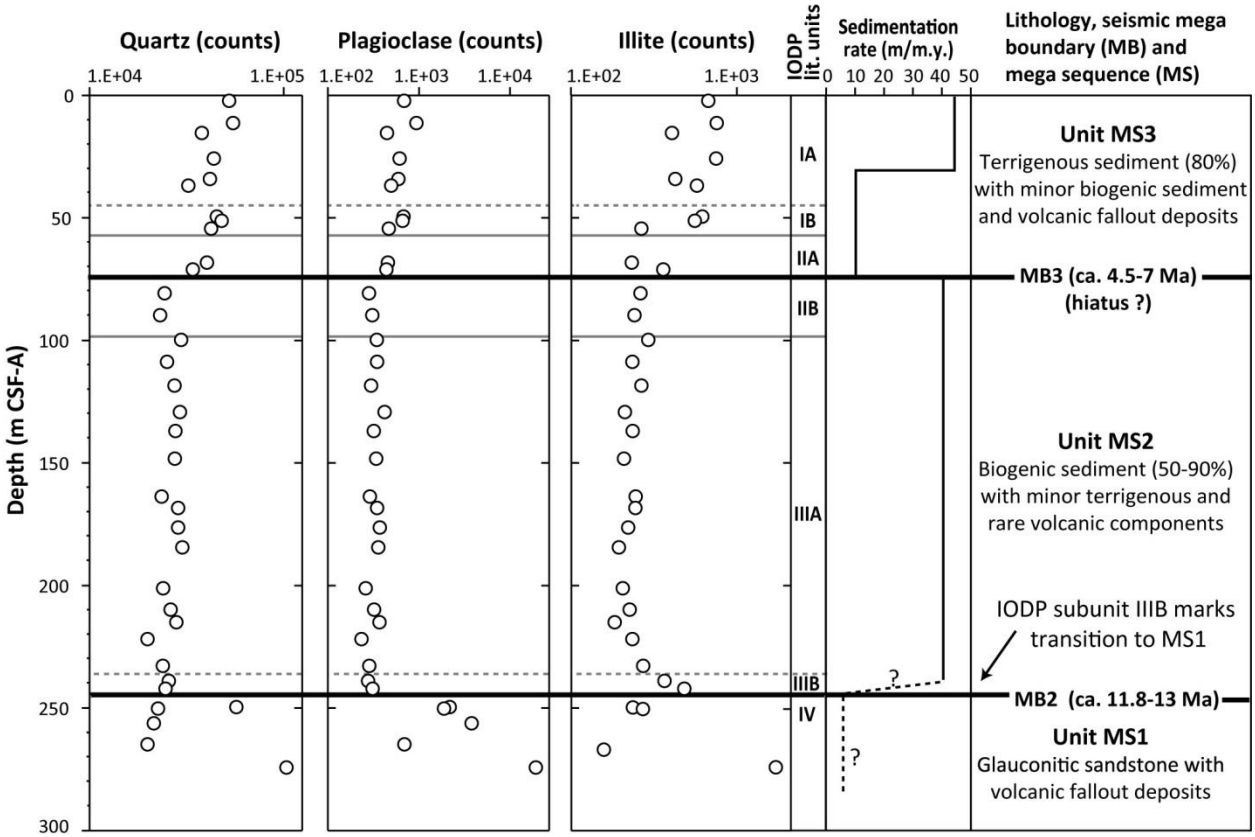
Quartz (counts)
Plagioclase (counts)
Illite (counts)
IODP lit. units
Sedimentation rate (m/m.y.)
Lithology, seismic mega boundary (MB) and mega sequence (MS)
1.E+04
1.E+05
1.E+02
1.E+03
1.E+04
1.E+02
1.E+03
0
10 20 30 40 50
Depth (m CSF-A)
0
50
100
150
200
250
300
IA
IB
IIA
IIB
IIIA
IIIB
IV
Unit MS3
Terrigenous sediment (80%) with minor biogenic sediment and volcanic fallout deposits
MB3 (ca. 4.5-7 Ma)
(hiatus ?)
Unit MS2
Biogenic sediment (50-90%) with minor terrigenous and rare volcanic components
IODP subunit IIIB marks transition to MS1
MB2 (ca. 11.8-13 Ma)
Unit MS1
Glauconitic sandstone with volcanic fallout deposits
?
?

Fig. 14

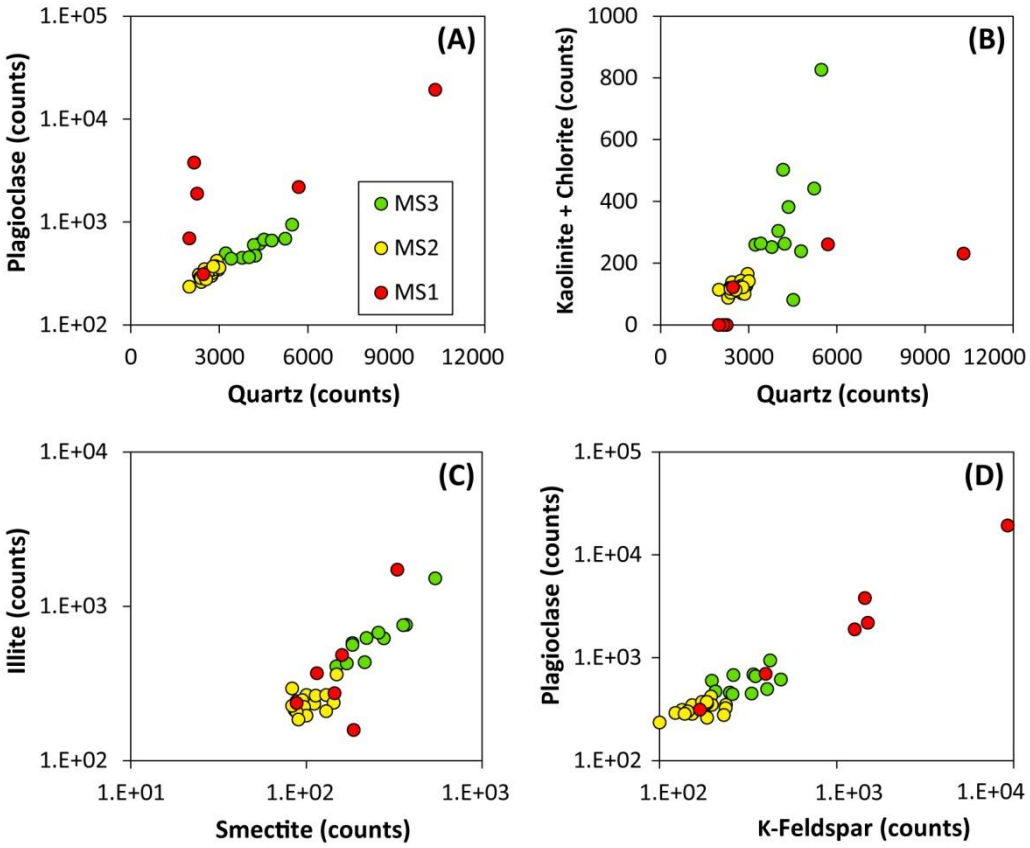
(A)
Plagioclase (counts)
Quartz (counts)
MS3
MS2
MS1
(B)
Kaolinite + Chlorite (counts)
Quartz (counts)
(C)
Illite (counts)
Smectite (counts)
(D)
Plagioclase (counts)
K-Feldspar (counts)

Fig. 15

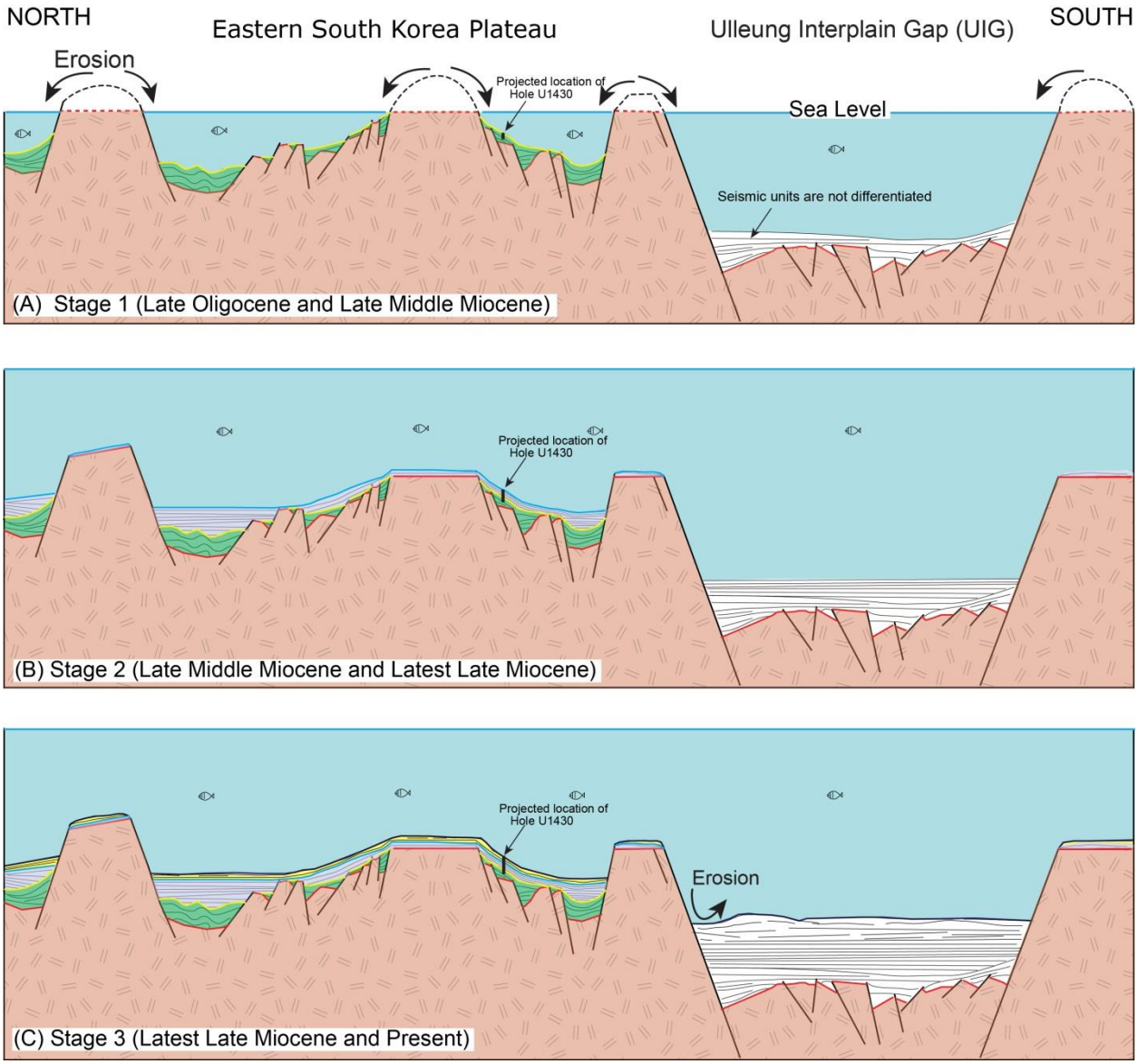
NORTH
Eastern South Korea Plateau
Ulleung Interplain Gap (UIG)
SOUTH
Erosion
Projected location of Hole U1430
Sea Level
Seismic units are not differentiated
(A) Stage 1 (Late Oligocene and Late Middle Miocene)
Projected location of Hole U1430
(B) Stage 2 (Late Middle Miocene and Latest Late Miocene)
Projected location of Hole U1430
Erosion
(C) Stage 3 (Latest Late Miocene and Present)

Tables

Table 1.

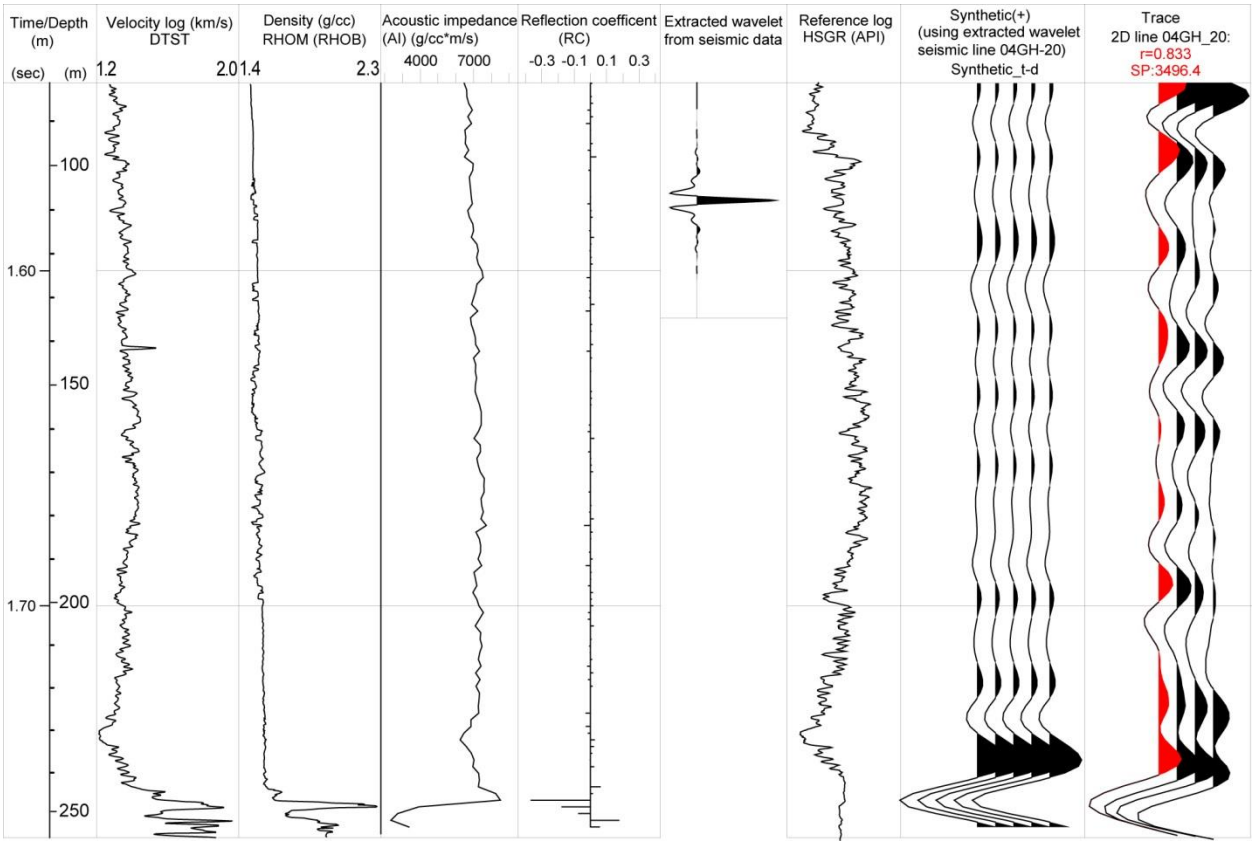

Table 2.

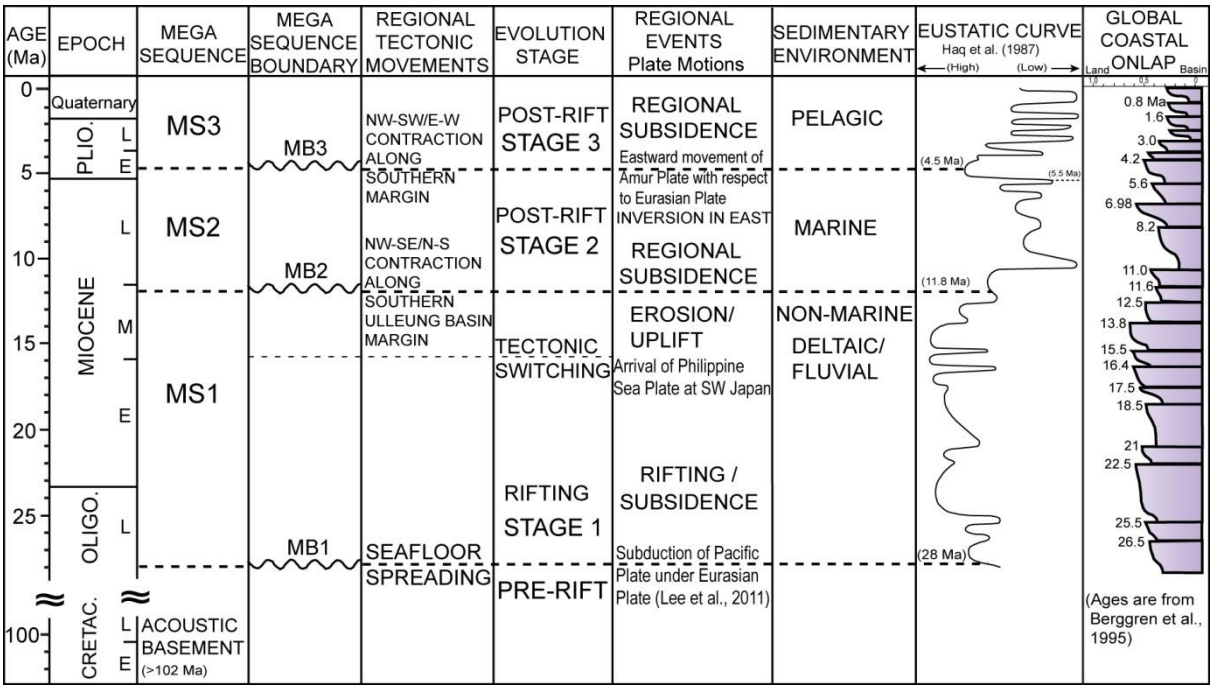
AGE (Ma)
EPOCH
MEGA SEQUENCE
MEGA SEQUENCE BOUNDARY
REGIONAL TECTONIC MOVEMENTS
EVOLUTION STAGE
REGIONAL EVENTS Plate Motions
SEDIMENTARY ENVIRONMENT
EUSTATIC CURVE
Haq et al. (1987)
(High)
(Low)
GLOBAL COASTAL ONLAP
Land
Basin
0
5
10
15
20
25
100
Quaternary
PLIO.
L
E
MIOCENE
L
M
E
OLIGO.
L
CRETAC.
L
E
MS3
MS2
MS1
ACOUSTIC BASEMENT
(>102 Ma)
MB3
MB2
MB1
NW-SW/E-W CONTRACTION ALONG SOUTHERN MARGIN
NW-SE/N-S CONTRACTION ALONG SOUTHERN ULLEUNG BASIN MARGIN
SEAFLOOR SPREADING
POST-RIFT STAGE 3
POST-RIFT STAGE 2
TECTONIC SWITCHING
RIFTING STAGE 1
PRE-RIFT
REGIONAL SUBSIDENCE
Eastward movement of Amur Plate with respect to Eurasian Plate
INVERSION IN EAST
REGIONAL SUBSIDENCE
EROSION/ UPLIFT
Arrival of Philippine Sea Plate at SW Japan
RIFTING / SUBSIDENCE
Subduction of Pacific Plate under Eurasian Plate (Lee et al., 2011)
PELAGIC
MARINE
NON-MARINE
DELTAIC/ FLUVIAL
(4.5 Ma)
(5.5 Ma)
(11.8 Ma)
(28 Ma)
0.8 Ma
1.6
3.0
4.2
5.6
6.98
8.2
11.0
11.6
12.5
13.8
15.5
16.4
17.5
18.5
21
22.5
25.5
26.5
(Ages are from Berggren et al., 1995)